Title

Brake System Modeling, Control And Integrated Brake/throttle Switching Phase I

Authors

Hedrick, Karl
Gerdes, J.C.
Maciuca, D.B.
et al.

Publication Date

1997

CALIFORNIA PATH PROGRAM
INSTITUTE OF TRANSPORTATION STUDIES
UNIVERSITY OF CALIFORNIA, BERKELEY

Brake System Modeling, Control and Integrated Brake/Throttle Switching: Phase I

J.K. Hedrick, J.C. Gerdes,
D.B. Maciuca, D. Swaroop
Universtiy of California, Berkeley

California PATH Research Report
UCB-ITS-PRR-97-21

This work was performed as part of the California PATH Program of the University of California, in cooperation with the State of California Business, Transportation, and Housing Agency, Department of Transportation; and the United States Department of Transportation, Federal Highway Administration.

Report for MOU 101

May 1997

ISSN 1055-1425

This paper uses Postscript Type 3 fonts. Although reading it on the screen is difficult it will print out just fine.

Brake System Modeling, Control and Integrated Brake/Throttle Switching Phase I

Final Report

Submitted to: PATH (MOU 237)

J.K. Hedrick
J.C. Gerdes
D.B. Maciuca
D. Swaroop

Mechanical Engineering Department
University of California at Berkeley
Berkeley, CA 94720-1740

Abstract

This report presents the findings obtained during the first year of a three year project concerned with the modeling and control issues regarding braking in an Intelligent Vehicles and Highway Systems (IVHS) environment. Specifically, the report addresses the issue of vehicle control in an automated highway system, brake actuation and coordinated brake and throttle switching.

Based on the data accumulated over the last years a fluidic model of the master cylinder and brake hydraulics was developed. A reduced model based on physical principles was achieved. This model explicitly describes the nonlinear capacitance of the brake system. Furthermore, the model allows for brake pressure variations between wheels. This will be used in the development of independent wheel control. Such a system is expected to provide stability during emergency braking and brake steer in a combined lateral/longitudinal vehicle. In order to obtain a complete model of a modern vehicle brake system, a reduced model of the vacuum booster was developed. Both models have been implemented in simulations and compared with experimental data. The results show a very high degree of correlation between the model and the actual brake system.

Having treated brake modeling and controller design in the past, we now turn attention towards applying these results to the vehicle control problem. Specifically, we seek a controller structure which can modulate the engine and brake torques as necessary to perform the four basic longitudinal control actions of speed control, spacing control, platoon joining and platoon splitting. This chapter approaches the design of such a structure from the standpoint of multiple-surface sliding control, in the spirit of previous work by (McMahon *et al.*, 1990) and others. The resulting controller consists of three elements: an "upper" surface controller dependent upon the longitudinal control task, a switching logic to choose between brake and throttle control and separate "lower" surface controllers for engine and brake torques. Under the formalism of multiple-surface sliding control, the upper surface controller is designed by assuming that the longitudinal vehicle acceleration may be controlled directly. Tracking this acceleration, which is designated a "synthetic input," subsequently becomes the control objective for the lower surface controllers. Intuitively, if the engine and brake dynamics are fast, relative to the desired acceleration, such decoupling of the design problem

produces acceptable performance.

Although there is a quasi-linear relationship between slave cylinder pressure and brake torque, that relationship varies with several parameters including, but not limited to, temperature, friction material and speed. Under these conditions, robustness can be achieved through the use of adaptive control algorithms. Lyapunov-based adaptive control algorithms were developed to compensate for the variation in friction coefficient between the brake rotors and brake pads. A thorough investigation of the available systems of direct brake torque measurement was performed. The winning solution is an instrumented brake rotor. The rotor deflection is measured using a set of strain gages. The measurement is then transmitted to the computer via a transmitter/receiver pair.

A method for designing stable controllers for uncertain, mismatched nonlinear systems is proposed. This method is similar to the one proposed by Swaroop, et.al. in that it is using multiple surface control methods with low pass filters included in the design. However, the method presented here uses nonsmooth control which has the benefit of reducing the final tracking error. Differential Inclusion theory is used to prove the stability of this controller. This methodology is applied to the control of brake systems in an automated highway environment. A simplified brake model taylored for control applications is used to illustrate the methodology. Simulation results show the feasibility of such technique.

Keywords: IVHS, AHS, AVCS, Longitudinal Control, Brake Control, Braking, Switched Control.

Executive Summary

Previous models of powertrain dynamics for control have not included the brakes, while dynamic models for braking have originated in the context of design. As a result, such models exhibit far too much complexity for controller development or simulation of an entire vehicle platoon. Others produced a rather comprehensive model of a complete brake system, yet required too many states to describe the dynamics of the pedal, vacuum booster, master cylinder and brake lines (collectively, the brake apply system).

Within the context of highway automation, brake dynamics have generally been considered to be a first-order linear system in conjunction with a pure time delay or transport lag. Based upon experimental results, a combined actuator and brake system model for AICC consisting of a linear, first-order system with amplitude-dependent parameters was devised. This model, however, was dominated by very slow actuator dynamics, exhibited limited accuracy and did not allow for analysis of individual components.

This report presents a three-state model of brake dynamics which, despite its simplicity, meets or exceeds the accuracy of previous models. Furthermore, aspects critical to control design, such as hysteresis and disturbance modeling are explicit in this formulation.

Successful longitudinal control of a vehicle in an Intelligent Vehicle and Highway System (IVHS) or Autonomous Intelligent Cruise Control (AICC) environment is highly dependent on the adequate control of the vehicle's subsystems. Most of those systems are highly nonlinear and include a wide range of uncertainties. A method for designing stable controllers for uncertain, mismatched nonlinear systems is proposed. This method is similar to the one proposed by Swaroop, et.al. in that it is using multiple surface control methods with low pass filters included in the design. However, the method presented here uses nonsmooth control which has the benefit of reducing the final tracking error. Differential Inclusion theory is used to prove the stability of this controller. This methodology is applied to the control of brake systems in an automated highway environment.

Having treated brake modeling and controller design in the past, we now turn attention towards applying these results to the vehicle control problem. Specifically, we seek a controller structure which can modulate the engine and brake torques as necessary to perform the four basic longitudinal con-

trol actions of speed control, spacing control, platoon joining and platoon splitting. This analysis approaches the design of such a structure from the standpoint of multiple-surface sliding control, in the spirit of previous work by (McMahon *et al.*, 1990) and others. The resulting controller consists of three elements: an "upper" surface controller dependent upon the longitudinal control task, a switching logic to choose between brake and throttle control and separate "lower" surface controllers for engine and brake torques. Under the formalism of multiple-surface sliding control, the upper surface controller is designed by assuming that the longitudinal vehicle acceleration may be controlled directly. Tracking this acceleration, which is designated a "synthetic input," subsequently becomes the control objective for the lower surface controllers. Intuitively, if the engine and brake dynamics are fast, relative to the desired acceleration, such decoupling of the design problem produces acceptable performance.

As described later, both the multiple-surface controller and the switching condition can be put into a broader mathematical framework. Within this framework, very rigorous guarantees of system performance can be derived and issues of gain selection and saturation treated explicitly. The true strengths of these mathematics, however, are the extent to which they can be applied to real systems with nonlinearities, uncertainties and neglected actuator dynamics and the intuitive design procedure that results. Accordingly, this chapter presents a physically intuitive approach to the problem of vehicle control which highlights the strengths of the theory developed in subsequent chapters.

A method to estimate the coefficient between the brake pressure at the wheel and the brake torque is presented. An experimental setup to directly measure the brake torque was is presented.

The basic longitudinal equation of vehicle motion present a simple two-state engine model based upon the work of (Moskwa and Hedrick, 1987) and (Cho and Hedrick, 1989). Based on these equations, a switching logic for coordinating the throttle and brake controllers and a means of determining the desired brake and engine torques is presented. In order to reduce potential chatter across the interface in implementation, a hysteresis element is added to this logic. The analysis concludes with simulation results validating the use of the coordinated control structure within the context of speed and spacing control.

Contents

List of Figures

List of Tables

Chapter 1

Introduction

This report presents the findings obtained during the first year of a three year project concerned with the modeling and control issues regarding braking in an Intelligent Vehicles and Highway Systems (IVHS) environment. Specifically, the report addresses the issue of vehicle control in an automated highway system, brake actuation and coordinated brake and throttle switching.

Chapter 2 presents a hydraulic model of the brake system which is the result of extensive experimental and simulation work. A reduced model based on physical principles was achieved. This model explicitly describes the nonlinear capacitance of the brake system. Furthermore, the model allows for brake pressure variations between wheels. The results show a very high degree of correlation between the model and the actual brake system.

Chapter 3 presents a method for designing stable controllers for uncertain, mismatched nonlinear systems. This method is similar to the one proposed by Swaroop, et.al. in that it is using multiple surface control methods with low pass filters included in the design. However, the method presented here uses nonsmooth control which has the benefit of reducing the final tracking error. Differential Inclusion theory is used to prove the stability of this controller. This methodology is applied to the control of brake systems in an automated highway environment.

Chapter 4 presents a method to estimate the coefficient between the brake pressure at the wheel and the brake torque. An experimental setup to directly measure the brake torque is also presented.

Chapter 5 seeks a controller structure which can modulate the engine

and brake torques as necessary to perform the four basic longitudinal control actions of speed control, spacing control, platoon joining and platoon splitting. This chapter approaches the design of such a structure from the standpoint of multiple-surface sliding control.

Chapter 6 summarizes the findings of this report.

Chapter 2

Brake System Modeling

From development to deployment, models of vehicle dynamics play a crucial role in all aspects of automated highway design. Within the context of brake control, modeling fills three distinct needs by providing a basis for hardware design and evaluation, control algorithm development and simulation. Since automotive braking systems (Figure 2.1) do not possess a unique actuation point comparable to the throttle input in engine control, the design of brake actuators is decidedly nontrivial. Dynamic models are therefore required to examine the tradeoffs between complexity and performance for actuation strategies ranging from a hydraulic cylinder attached to the pedal linkage to modulation of a traction control system. The choice of actuation strategy, in turn, determines which components are enclosed by the feedback loop or, equivalently, which component models combine to form the plant model for controller development. Finally, since evaluation of controllers on the test track is an expensive proposition, this plant model should be capable of providing an accurate simulation from which performance can be estimated prior to experimental validation. To fulfill these three objectives simultaneously, a good model should therefore make control problems (such as nonlinearities, disturbances or uncertainty) explicit, provide sufficient fidelity for simulation and yet be simple enough to provide a basis for model-based controllers.

Unfortunately, existing vehicle models fail to satisfy one or more of these criteria. Previous models of powertrain dynamics for control have not included the brakes (Cho and Hedrick, 1989), while dynamic models for braking have originated in the context of design. As a result, such models

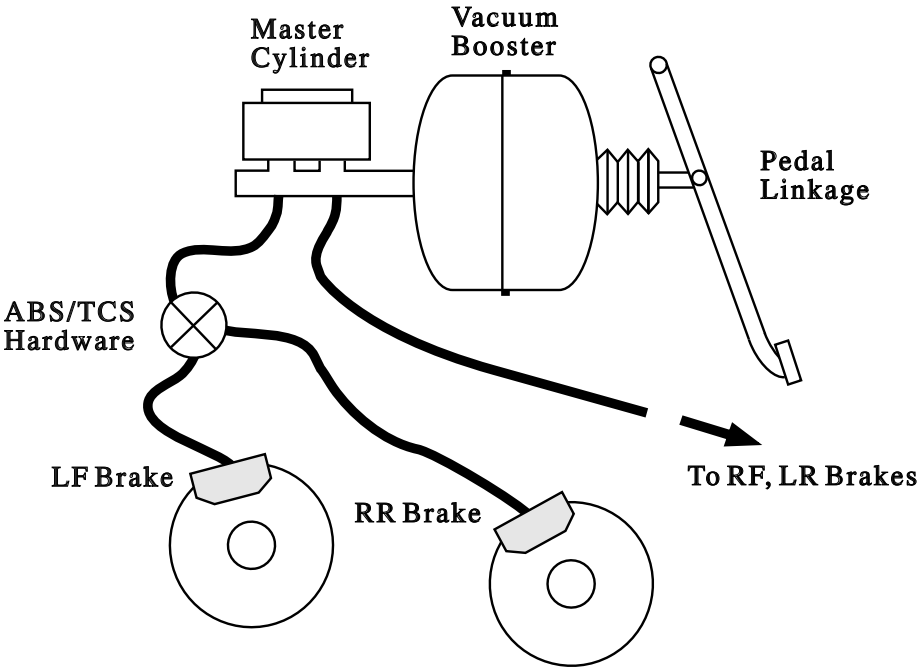

Figure 2.1: Brake System Components

exhibit far too much complexity for controller development or simulation of an entire vehicle platoon. (Fisher, 1970) produced a rather comprehensive model of a complete brake system, yet required 18 states to describe the dynamics of the pedal, vacuum booster, master cylinder and brake lines (collectively, the brake apply system). (Khan *et al.*, 1994) updated and streamlined this model for the dynamics of the apply system, but still included 10 states and validated the model only for very slow brake applications. In addition, this model contained some highly questionable thermodynamics and ignored reaction washer hysteresis and master cylinder seal friction, which both impact on closed-loop control.

Within the context of highway automation, brake dynamics have generally been considered to be a first-order linear system in conjunction with a pure time delay or transport lag (McMahon *et al.*, 1990). Based upon experimental results, (Raza *et al.*, 1994) devised a combined actuator and brake system model for AICC consisting of a linear, first-order system with amplitude-dependent parameters. This model, however, was dominated by very slow actuator dynamics, exhibited limited accuracy and did not allow for analysis of individual components. (Gerdes *et al.*, 1993), in an earlier version of this work, produced a dynamic model with five states, but were unable to fully capture certain aspects of the brake hydraulics or the hysteresis behavior of the vacuum booster.

This chapter presents a three-state model of brake dynamics which, despite its simplicity, meets or exceeds the accuracy of previous models. Furthermore, aspects critical to control design, such as hysteresis and disturbance modeling are explicit in this formulation. Section 2.1 provides an overview of hydraulic system operation and develops a four-state model of the brake hydraulics. Within the context of longitudinal control, this model is reduced to a two-state version and, finally, a one-state nonlinear model. While the model does not specifically include ABS operation (because of both the focus on amplitude braking and the fact that ABS hardware and algorithms are system-dependent), it is flexible enough that such systems may be added. Indeed, at least one reference (van Zanten *et al.*, 1995) indicates that this model is compatible with models used for ABS design in industry. The results of extensive experimental validation follow, along with several notes regarding the applicability of this model to different vehicles and the implications of the model for actuator design.

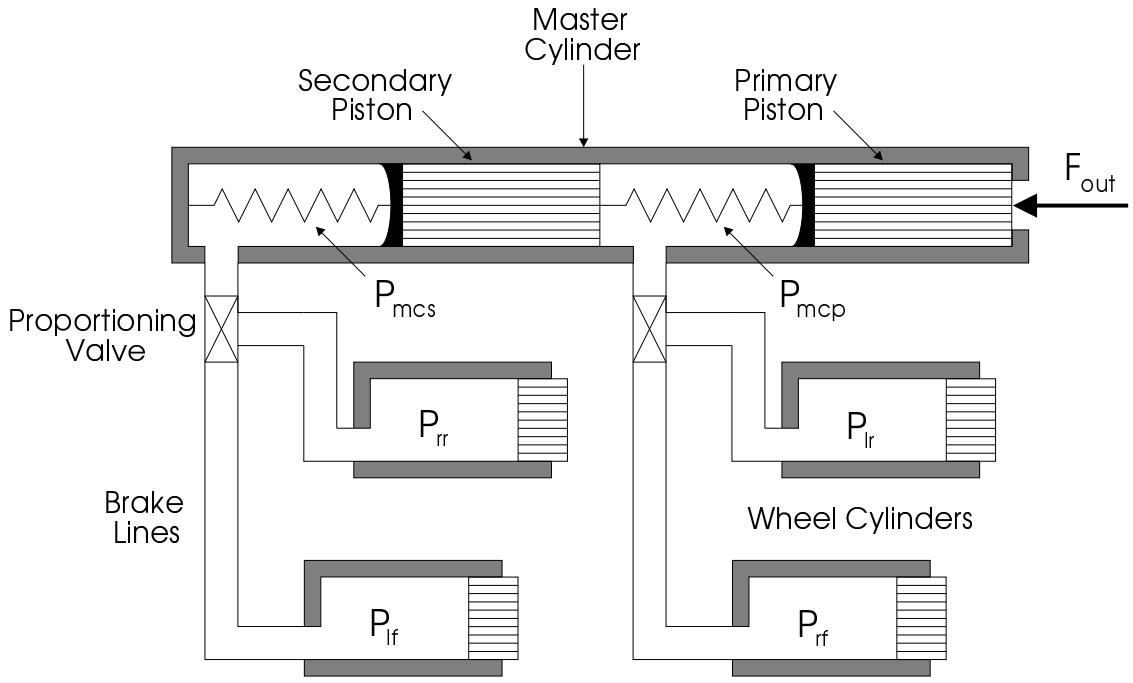

Figure 2.2: Schematic of Brake Hydraulic System

2.1 Brake System Hydraulics

The brake hydraulics (illustrated schematically in the absence of ABS hardware by Figure 2.2) play three major roles during braking. First, they serve as a convenient means of force transfer and amplification between the driver input (after the vacuum booster amplification) and the actual friction elements. Prior to the introduction of hydraulics by Deusenberg, this task had to be accomplished through mechanical linkages (Puhn, 1985). Secondly, the design of modern hydraulic systems, with two concentric pistons in the master cylinder, serves a safety function. As will be discussed in Section 2.1.1, this design allows for some braking even in the event of a catastrophic failure in one of the circuits. Finally, the hydraulics work to maintain vehicle stability through the proportioning valve operation. This element increases the relative braking on the front wheels at higher levels of deceleration, compensating for vehicle weight transfer and preventing premature rear-wheel lockup. The following sections discuss each of these components

individually and develop dynamic models of their operation.

2.1.1 Master Cylinder

Modern tandem master cylinders contain primary and secondary pistons arranged concentrically in a single bore. As illustrated in Figure 2.2, this construction serves to separate the brake hydraulics into two separate circuits. In most modern cars, this separation involves a diagonal split (with each circuit containing a front brake and the rear brake on the opposite side of the car), although front-rear splits are also possible. The rationale behind the diagonal split is purely related to vehicle stability and safety. In the event of a rupture in one of the hydraulic circuits, the piston is designed to "bottom out" against either the master cylinder or the other piston, ensuring that the force is still transmitted to the intact circuit (Puhn, 1985). In such cases, a diagonal split ensures that this braking will be split both between the axles (to prevent lock-up) and between the right and left sides (to enhance lateral stability).

In addition, the master cylinder construction must ensure that the brake lines remain filled with fluid and free of air bubbles. This task is complicated by the fact that the fluid capacity of the brake system changes as the pads wear. By opening the brake lines to a fluid reservoir upon release, however, the lines remain fully charged with fluid without any residual pressure or brake drag. Traditionally, this task was accomplished by a compensating port (shown in Figure 2.3) which was covered during brake application and opened upon release as the return springs pushed the pistons back to their initial positions. With the advent of ABS, however, such designs were not always feasible (since the ABS modulation could force the seal back over the port under pressure, damaging the seal (Buschmann *et al.*, 1993)) so the central-valve master cylinder was developed. With this construction, shown in Figure , the pistons contain small valves which open when the pistons are pressed back against stops in the bore and connect the brake lines to the reservoir.

These flows, however, have little effect upon the behavior of brakes during application. As a result, we consider the master cylinder to consist of two sealed circuits which transform an input force to pressure and allow flow only into the brake lines. Neglecting the small inertias of the pistons, the pressure

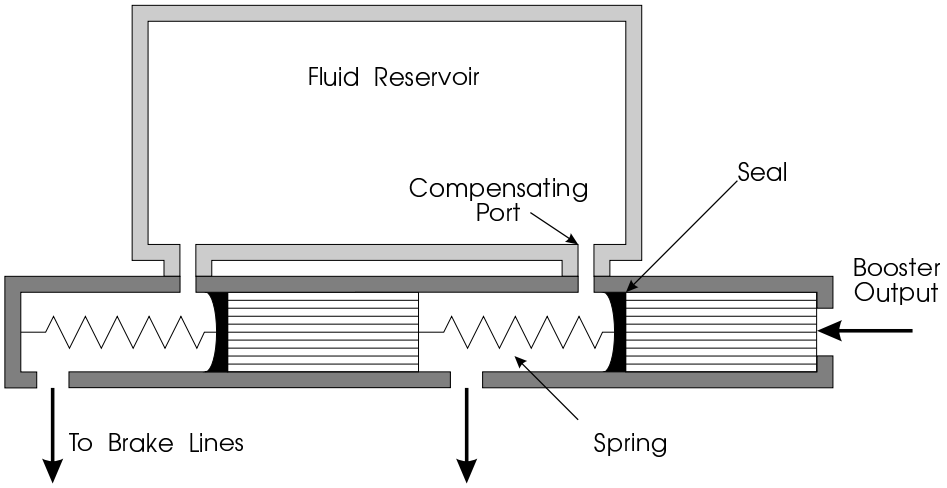

Figure 2.3: Compensating Port Type Master Cylinder

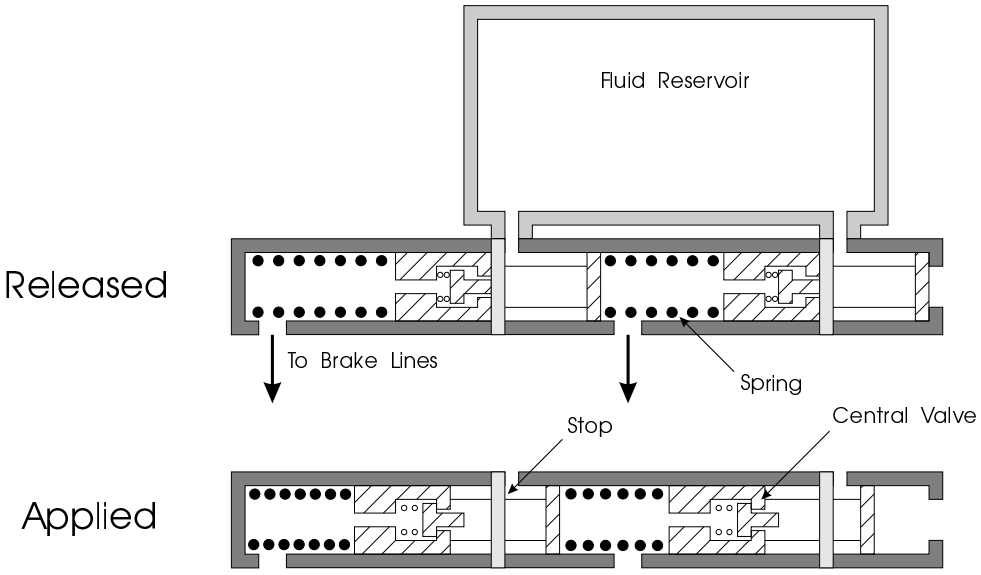

Figure 2.4: Central Valve Type Master Cylinder

in each circuit is given by:

$$P_{mcp} = (F_{out} - F_{csp} - F_{cfp}) / A_{mc} \quad (2.1)$$
$$P_{mcs} = P_{mcp} - (F_{css} + F_{cfs}) / A_{mc} \quad (2.2)$$

where F_{csp} and F_{css} are the return spring forces and F_{cfp} and F_{cfs} are the seal friction forces for the primary and secondary cylinders, respectively. For nonzero displacements, the spring forces are given by:

$$F_{csp} = F_{csp_o} + K_{csp}(x_{mcp} - x_{mcs}) \quad (2.3)$$
$$F_{css} = F_{css_o} + K_{css} x_{mcs} \quad (2.4)$$

where x_{mcp} and x_{mcs} represent the displacements of the pistons. In terms of the variable x_{pp},

$$x_{pp} = \begin{cases} x_{mcp} & F_{out} > 0 \\ 0 & \text{otherwise} \end{cases} \quad (2.5)$$

The seal friction is assumed here to follow a Coulomb friction model (which requires a hysteresis or memory element to implement in simulation). In reality, the friction increases somewhat at higher pressures due to the construction of the cup-type seal. This behavior can easily be added to the model if so desired.

2.1.2 Proportioning Valves

When a vehicle brakes, weight is transferred dynamically to the front wheels. Since each tire can support only a certain *ratio* of braking force to normal force before lock-up (often referred to as the "peak friction coefficient," though this is somewhat poor terminology), braking should shift to the front wheels to compensate for this weight transfer. To perfectly compensate for weight transfer, the braking shift should follow a parabolic curve though, in practice, a bilinear approximation is used. This bilinear proportioning of brake force is accomplished by the proportioning valve, which begins to function only after a threshold, or "knee" pressure is reached. Below the knee, then, the front and rear pressures are identical, but above the knee pressure, the proportioning valve limits the rear pressure rise to counteract the weight transfer. A complementary element of the brake hydraulics is the metering valve which prevents flow to the front brakes below a certain

pressure. This valve is incorporated into some rear-wheel drive cars with front discs and rear drums to prevent the discs from assuming all braking at low decelerations (Limpert, 1992).

Physically, proportioning valve construction is similar to that illustrated in Figure 2.5 (several cross-sections of actual valves can be found in (Limpert, 1992)). The bilinear pressure results from the unequal upstream and downstream piston areas and the pre-load in the return spring. At low pressures,

$$P_u A_u + F_{ps} \geq P_d A_d \tag{2.6}$$

the piston remains pushed against stops to the left and fluid is free to flow through the valve. Hence, neglecting any flow restriction, the upstream and downstream pressures are equal. At the knee pressure, however,

$$P_k A_u + F_{ps} = P_k A_d \tag{2.7}$$

and any further increase in upstream pressure, δP_u, results in a corresponding increase in downstream pressure of only $\delta P_d = \left(\frac{A_u}{A_d}\right) \delta P_u$. When the upstream pressure decreases, the valve inside the piston opens, allowing fluid to drain and the downstream pressure to decrease.

Because of seal friction in the valve and the difficulty of matching springs and areas so that the release behavior exactly equals the apply behavior, hysteresis exists in proportioning. This can be made quite small in practice (Nash, 1983), however, so it is neglected in this analysis. Furthermore, the proportioning valves are assumed to be mounted integrally with the master cylinder so that flow between the master cylinder and valve can be ignored. As a result, the upstream pressures are simply given by the primary and secondary master cylinder pressures.

Taking into account metering and proportioning, therefore, the pressures immediately downstream of this valve are:

$$P_{prf} = \begin{cases} 0 & P_{mcp} \leq P_m \\ P_{mcp} - P_m & \text{otherwise} \end{cases} \tag{2.8}$$

$$P_{plr} = \begin{cases} P_{mcp} & P_{mcp} \leq P_k \\ P_k + (\frac{A_u}{A_d})(P_{mcp} - P_k) & \text{otherwise} \end{cases} \tag{2.9}$$

$$P_{prr} = \begin{cases} 0 & P_{mcs} \leq P_m \\ P_{mcs} - P_m & \text{otherwise} \end{cases} \tag{2.10}$$

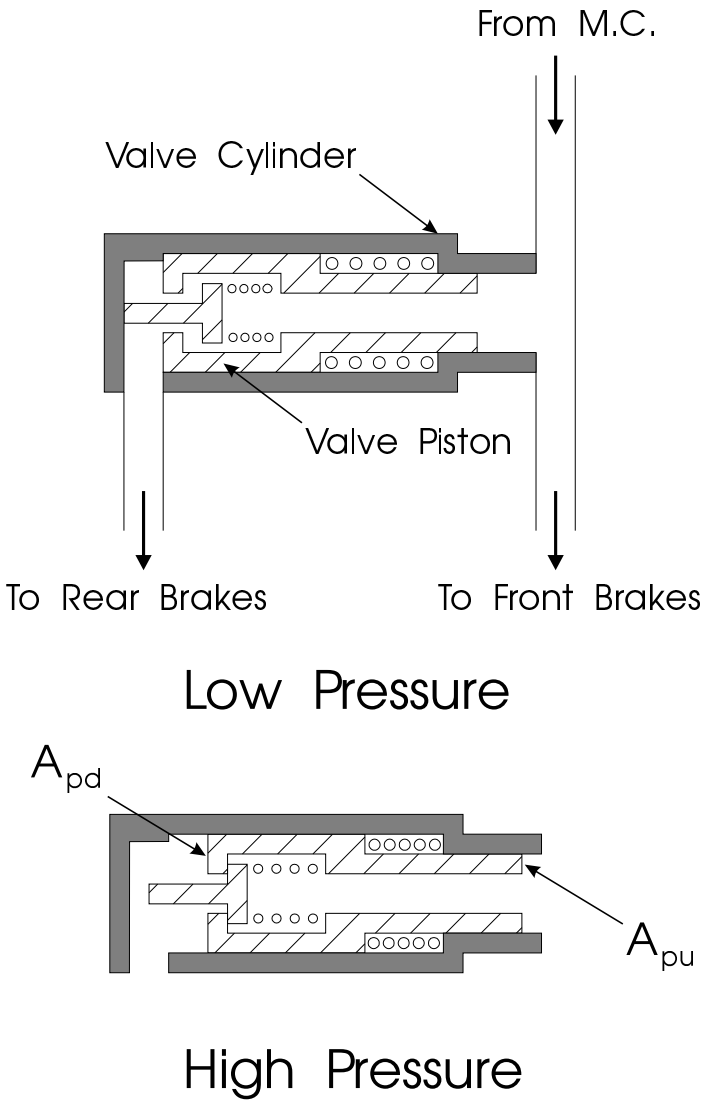

Figure 2.5: Proportioning Valve Operation

$$P_{plf} = \begin{cases} P_{mcs} & P_{mcs} \leq P_k \\ P_k + (\frac{A_w}{A_d})(P_{mcs} - P_k) & \text{otherwise} \end{cases} \quad (2.11)$$

P_m represents the pressure at which the metering valve releases pressure to the front wheels, so if no metering valve is used, clearly, $P_m = 0$.

2.1.3 Brake Lines and Wheel Cylinders

Finally, we are able to derive the state equations for the brake hydraulics. One of the limitations of the original model by (Gerdes *et al.*, 1993) was the approximation of the brake hydraulics by a linear, first-order system. In this work, the hydraulics are modeled from fundamental principles by assuming incompressible flow. The state variables are accordingly taken to be the volume of fluid displaced into each wheel cylinder, V_{rf}, V_{lr}, V_{lf} and V_{rr} or, compactly, V_α where $\alpha \in \{rf, lr, lf, rr\}$. In terms of the displacements used to calculate the return spring forces,

$$x_{mcs} = (V_{lf} + V_{rr})/A_{mc} \quad (2.12)$$

$$x_{mcp} = (V_{rf} + V_{lr})/A_{mc} + x_{mcs} \quad (2.13)$$

The choice of these volumes as the state variables reflects the fact that pressure changes at the master cylinder are not immediately manifested at the wheels. Rather, fluid must flow to the wheels before the pressure there can increase.

The final aspect of the hydraulic model, therefore, involves relating the wheel pressure to the displaced fluid volume. To do this, the brake lines and wheel cylinders are assumed to possess some fluid capacity, allowing pressure at each wheel to be written:

$$P_{w\alpha} = P_{w\alpha}(V_\alpha) \qquad \alpha \in \{rf, lr, lf, rr\} \quad (2.14)$$

The general shape of this relationship for a brake is shown in Figure 2.6. Such shapes are, in general, characteristic of brake system hydraulics (Buschmann *et al.*, 1993). After an initial flow without pressure increase (caused by expansion in the lines and wheel cylinder seals and "knockback" of the caliper), the capacity may be approximated by a smooth function.

Then, flow to each wheel is modeled by Bernoulli's equation, giving state equations for the four hydraulic states. In terms of the pressures after

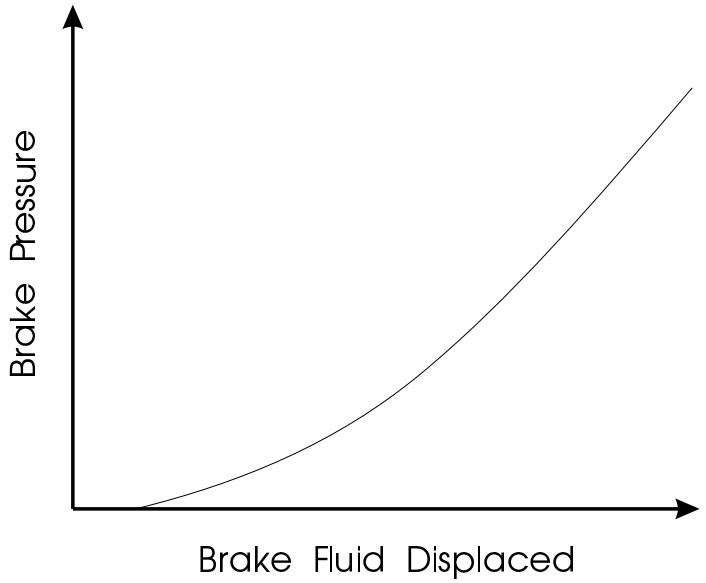

Figure 2.6: General Form for Brake Fluid Capacity

proportioning and metering, these equations are:

$$\dot{V}_{rf} = \sigma_{rf} C_{qrf} \sqrt{|P_{prf} - P_{wrf}|} \tag{2.15}$$

$$\dot{V}_{lr} = \sigma_{lr} C_{qlr} \sqrt{|P_{plr} - P_{wlr}|} \tag{2.16}$$

$$\dot{V}_{lf} = \sigma_{lf} C_{qlf} \sqrt{|P_{plf} - P_{wlf}|} \tag{2.17}$$

$$\dot{V}_{rr} = \sigma_{rr} C_{qrr} \sqrt{|P_{prr} - P_{wrr}|} \tag{2.18}$$

where

$$\sigma_{rf} = \text{sgn}\,(P_{prf} - P_{wrf}) \tag{2.19}$$

$$\sigma_{lr} = \text{sgn}\,(P_{plr} - P_{wlr}) \tag{2.20}$$

$$\sigma_{lf} = \text{sgn}\,(P_{plf} - P_{wlf}) \tag{2.21}$$

$$\sigma_{rr} = \text{sgn}\,(P_{prr} - P_{wrr}) \tag{2.22}$$

and $C_{q\alpha} (\alpha \in \{rf, lr, lf, rr\})$ denote flow coefficients for the various brake lines.

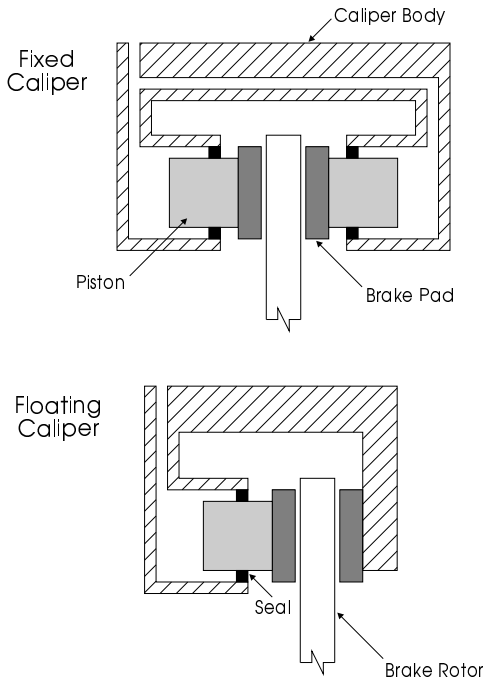

Figure 2.7: Brake Caliper Designs

2.1.4 Brakes and Pads

The remaining aspect of the model involves the transformation from wheel cylinder pressure to brake torque. Each wheel cylinder forms part of either a caliper brake (Figure 2.7) or a drum brake (shown in Figure 2.8), which translate the pressure into a force on a friction pad. The resulting frictional force between the pad and the rotor or drum produces the braking torque.

Since the inertia of the shoes or calipers are small, relative to the forces involved, we incorporate a static model.

$$\tau_{b\alpha} = \begin{cases} K_{b\alpha}\left(P_{w\alpha} - P_{po\alpha}\right) & P_{w\alpha} \geq P_{po\alpha} \\ 0 & \text{otherwise} \end{cases} \qquad \alpha \in \{rf, lr, lf, rr\} \tag{2.23}$$

where $K_{b\alpha}$ denotes the brake gain or "brake effectiveness" (Radlinski, 1991) and $P_{po\alpha}$ a "push-out" pressure below which the pads do not contact and no braking occurs. Physically, this pressure corresponds to the force needed to overcome the return springs in a drum brake or the caliper seal rollback in a disc brake.

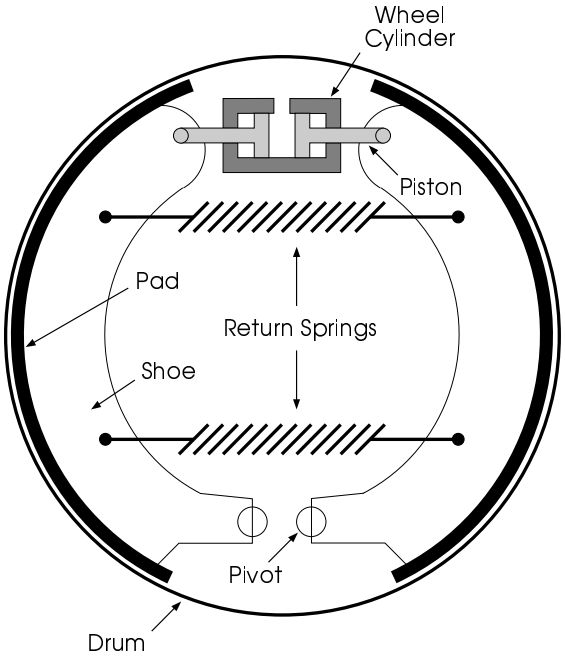

Figure 2.8: Drum Brake Construction

The brake effectiveness is, of course, composite of several factors including the frictional coefficient, the effective radius at which the force acts and, in the case of a drum brake, the servo effect. The composite form is used here deliberately, however, because of the difficulty of associating a single value of the brake gain with a particular brake. Indeed, the friction coefficient not only varies according to the wheel speed and brake pad temperature, but also across identically manufactured brake pads (Radlinski, 1991). Modeling such effects, however, requires considerable detail and produces only mediocre correlation (Gillespie, 1992). As a result, we propose this linear form with the understanding that $K_{b\alpha}$ is highly uncertain and subject to variation.

2.1.5 Reduced Order Models

The model presented above is quite general and rather comprehensive, enabling analysis of braking at each individual wheel. Furthermore, proportioning effects are made explicit and ABS operation may be included by allowing the ABS hardware to contribute to the fluid flow to the wheels in Equations 2.15 to 2.18. (van Zanten *et al.*, 1995), in fact, indicate that a similar model is used by Bosch in just such an application. Of course, analysis of high frequency oscillations in the brake fluid as a result of ABS operation requires a more detailed fluid model that includes compressibility and transmission line behavior.

For many aspects of vehicle control on an automated highway, however, even the level of detail presented here is unnecessary. Variations across wheels are not as important as the total amount of braking produced for pure longitudinal motion and neither ABS nor proportioning come into play at the low levels of deceleration associated with routine maneuvers on an automated highway (below, say, about 0.2g). As a result, the model can be simplified dramatically by including only one or two hydraulic states. These model reductions have physical interpretations which are discussed in the following sections.

Two-State Model

The most obvious simplification is to consider only the pressure change in each circuit and not the behavior of the individual wheels. Such a model is demonstrated in Figure 2.9. In this analysis, the two states become the fluid

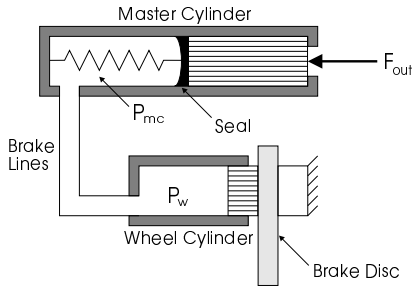

Single Circuit Model

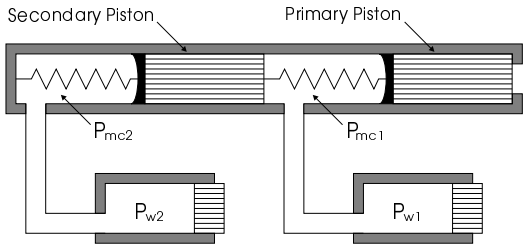

Dual Circuit Model

Figure 2.9: Reduced Order Hydraulic Models

volumes displaced into the primary and secondary circuits, V_p and V_s. The displacements, x_{mcp} and x_{mcs}, are then

$$x_{mcs} = V_s/A_{mc} \tag{2.24}$$
$$x_{mcp} = V_p/A_{mc} + x_{mcs} \tag{2.25}$$

The two state equations for V_p and V_s become:

$$\dot{V}_p = \sigma_p C_{qp}\sqrt{|P_{mcp} - P_{wp}|} \tag{2.26}$$
$$\dot{V}_s = \sigma_p C_{qs}\sqrt{|P_{mcs} - P_{ws}|} \tag{2.27}$$

where the master cylinder pressures are still given by Equations 2.1 and 2.2. Each circuit has its own fluid capacity

$$P_{wp} = P_{wp}(V_p) \tag{2.28}$$
$$P_{ws} = P_{ws}(V_s) \tag{2.29}$$

representing the composite fluid capacity of the two brakes on the circuit. The pressure split between front and rear can then be determined from a static proportioning relationship, if desired, though this modification is more appropriate below the level at which proportioning occurs. The brake torque is analogously found for each circuit:

$$\tau_{bp} = \begin{cases} K_{bp}(P_{wp} - P_{pop}) & P_{wp} \geq P_{pop} \\ 0 & \text{otherwise} \end{cases} \tag{2.30}$$

$$\tau_{bs} = \begin{cases} K_{bs}(P_{ws} - P_{pos}) & P_{ws} \geq P_{pos} \\ 0 & \text{otherwise} \end{cases} \tag{2.31}$$

Such simplifications are obviously most accurate when the two brakes can be modeled as a single equivalent brake. In other words, this implies that the variations in flow coefficients and push-out pressures are not particularly great.

Single State Model

Since this model is intended primarily as a tool for designing AICC or platooning strategies, the focus leans towards the development of brake force

as a whole, rather than the distribution of this force among individual wheels. Figure 2.9 schematically illustrates the hydraulic model as a single equivalent brake connected to the master cylinder. At the low brake applications required by platooning algorithms, where proportioning does not occur, this simplified model produces a good representation of the dynamics from the master cylinder to vehicle deceleration.

In this model, the output of the vacuum booster, after overcoming the master cylinder spring pre-load, F_{cso}, and seal friction, F_{cf}, is reflected as pressure in the master cylinder, P_{mc}:

$$P_{mc} = (F_{out} - F_{cs} - F_{cf})/A_{mc} \tag{2.32}$$

where A_{mc} represents the area of the master cylinder. Hence, for this model simplification to be accurate, the other forces on the secondary piston, F_{css} and F_{cfs}, should be small. The displacement, $x_{mcp} = x_{mc}$, is given by

$$x_{mc} = V/A_{mc} \tag{2.33}$$

where V is the volume of displaced brake fluid.

The state equation for the flow may be modeled from Bernoulli's equation:

$$\dot{V} = \sigma C_q \sqrt{|P_{mc} - P_w|} \tag{2.34}$$

where C_q is the effective flow coefficient and $\sigma = \text{sgn}\,(P_{mc} - P_w)$. The wheel cylinder is modeled as the lumped fluid capacity of the entire brake system:

$$P_w = P_w\,(V) \tag{2.35}$$

The cubic polynomial function representing this capacity is illustrated in Figure 2.10 along with some of the experimental data used to obtain it. The braking is then assumed to follow from this pressure:

$$\tau_b = \begin{cases} K_b\,(P_w - P_{po}) & P_w \geq P_{po} \\ 0 & \text{otherwise} \end{cases} \tag{2.36}$$

Figure 2.11 illustrates the experimentally determined torque/pressure relationship used to verify the appropriateness of a linear model. These results were obtained from moving tests by measuring vehicle deceleration and compensating for drag forces.

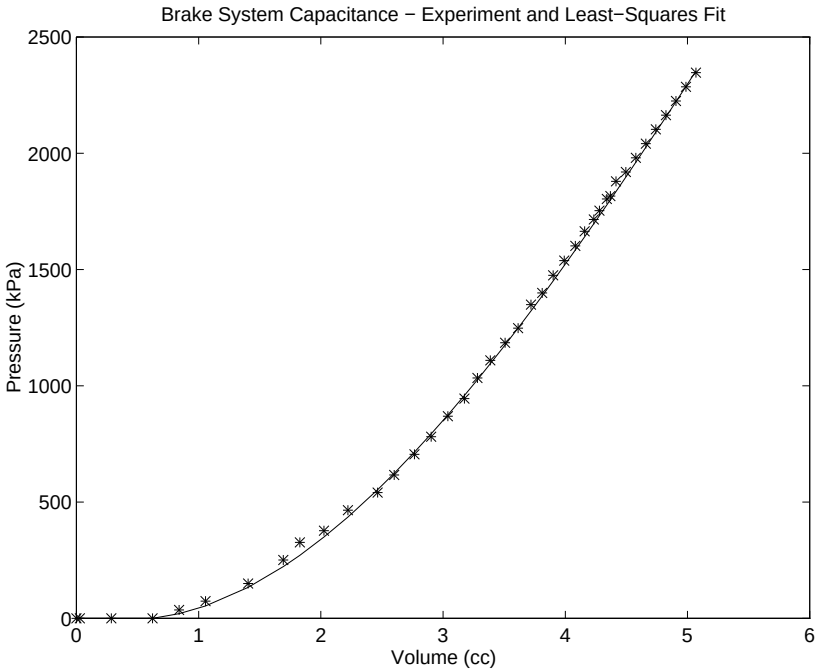

Figure 2.10: Brake System Capacitance

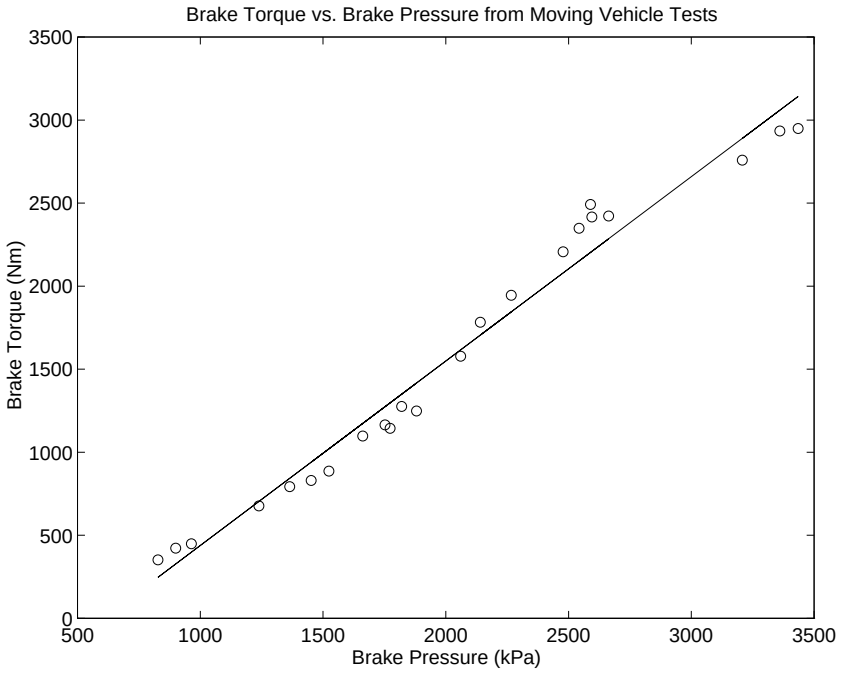

Figure 2.11: Brake Torque vs. Brake Pressure

2.1.6 Disturbance Modeling

When wear produces non-uniformities in the brake rotors or drums, pulsations in wheel cylinder pressure can appear at the frequency of wheel rotation and propagate to the master cylinder. Disturbances of this type were noted by (Gerdes *et al.*, 1993) and also appeared in experimental results by (Xu and Ioannou, 1992). Such effects are difficult to model accurately in a linear first-order approximation, but may be included explicitly as part of the nonlinear fluid capacity. Given a rotor non-uniformity of amplitude $d(\theta)$, where θ denotes the wheel angle of rotation, Equation 2.35 becomes:

$$P_w = P_w \left(V + A_{wc} d \left(\theta \right) \right) \tag{2.37}$$

where A_{wc} is the effective wheel cylinder area. This analysis can be applied to the 1-state, 2-state or 4-state models.

2.2 Experimental Validation

In order to validate the dynamic model and determine parameters such as the linearized flow coefficients, a series of tests was performed on the brake system of a test vehicle associated with the California PATH Program. This car was instrumented with pressure sensors in the apply and vacuum chambers, the intake manifold, the secondary brake line at the master cylinder and the front brake on the same hydraulic circuit. In addition, potentiometers were alternately attached to the pedal linkage and master cylinder to determine the displacements, x_{pr} and x_{mc}. A hydraulic cylinder attached to the pedal linkage supplied the input force. Where possible, parameters were determined directly by experiment; others were determined by matching simulation and experiment (see Table 2.1).

Figure 2.12 shows the results of the single-state brake hydraulic model considered as an individual element. To obtain these results, the measured master cylinder pressure from a step response test was used as an input to the model. As illustrated, the measured pressure at the wheel is almost identical to that predicted by the model. Repeating this test for a variety of apply rates and pressure magnitudes produced similar results. The only discrepancy noted with this model was for extremely slow apply rates where the primary circuit filled with fluid before the pressure was sufficient to

$F_{rso} = 97\ N$	$C_{aa} = 5.8 \times 10^{-5}\ m \cdot s$
$K_{rs} = 2411\ N/m$	$C_{av} = 2.2 \times 10^{-4}\ m \cdot s$
$F_{cso} = 138\ N$	$C_{vm} = 1.26 \times 10^{-4}\ m \cdot s$
$K_{cs} = 175\ N/m$	$\bar{C}_{leak} = 1.4 \times 10^{-7}\ m \cdot s$
$F_{app} = 50\ N$	$V_{vo} = 2.4 \times 10^{-3}\ m^3$
$F_{rel} = 50\ N$	$V_{ao} = 4.3 \times 10^{-4}\ m^3$
$F_{cf} = 80\ N$	$P_o = 10.67\ kPa$
$A_{mc} = 4.91 \times 10^{-4}\ m^2$	$C_q = 1.4\ cm^3/s\sqrt{kPa}$
$A_d = 5.33 \times 10^{-2}\ m^2$	

Table 2.1: Parameters Used in Brake System Simulations

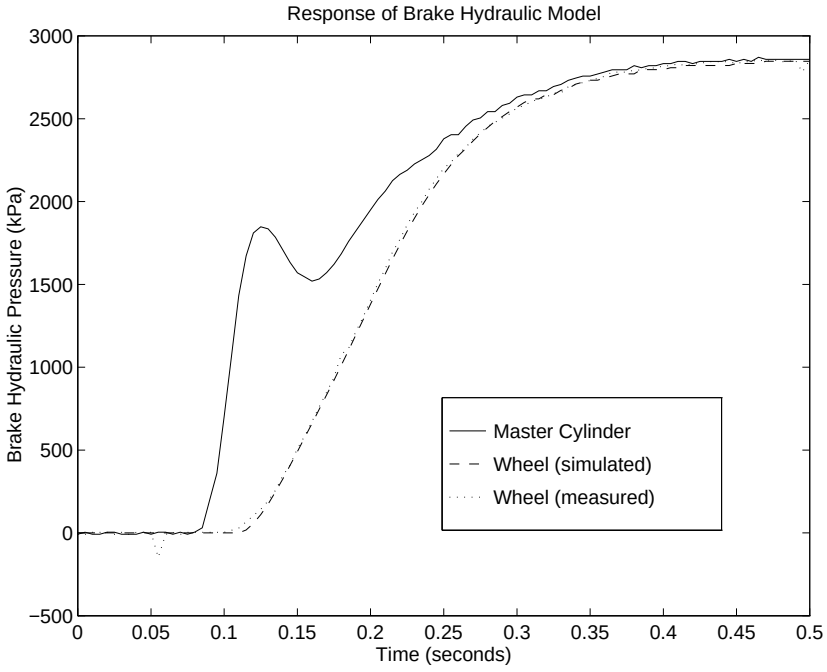

Figure 2.12: Validation of Brake Hydraulic Model

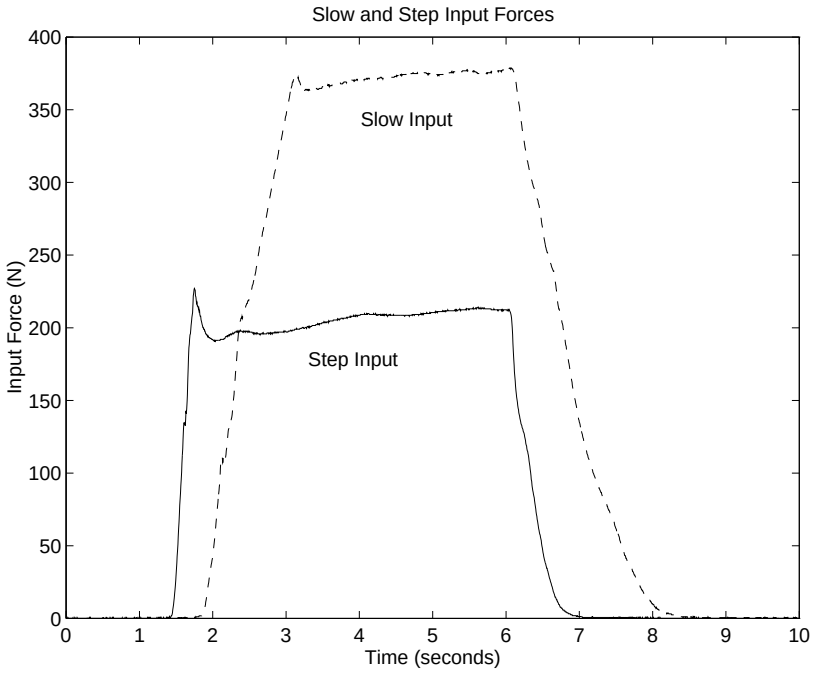

Figure 2.13: Input Forces Used in Simulations

overcome secondary seal friction. In such cases the simulation tended to slightly lead the experimental pressure rise.

Figure 2.13 shows two of the inputs used to validate the three-state model: a low amplitude step and a higher amplitude comparable to a human apply rate. As Figures 2.14 to 2.17 suggest, the correlation between simulation and experiment is quite high, even over a wide range of apply rates and amplitudes. Furthermore, those discrepancies that do exist may be clearly traced to modeling simplifications. In particular, the chamber pressures in Figures 2.14 and 2.16 show minor deviations from experiment as a result of linearization and the simplified treatment of orifice size and check valve flow. Qualitatively, however, simulation and experiment exhibit the same characteristics, implying that no significant behavior has been excluded. The effect of neglecting the booster inertia can be seen at the initiation of air flow. Since pedal inertia contributes to F_{in}, no single value for the booster characteristic can predict the exact force required to initiate braking for step and slow responses. Overall, this effect is small.

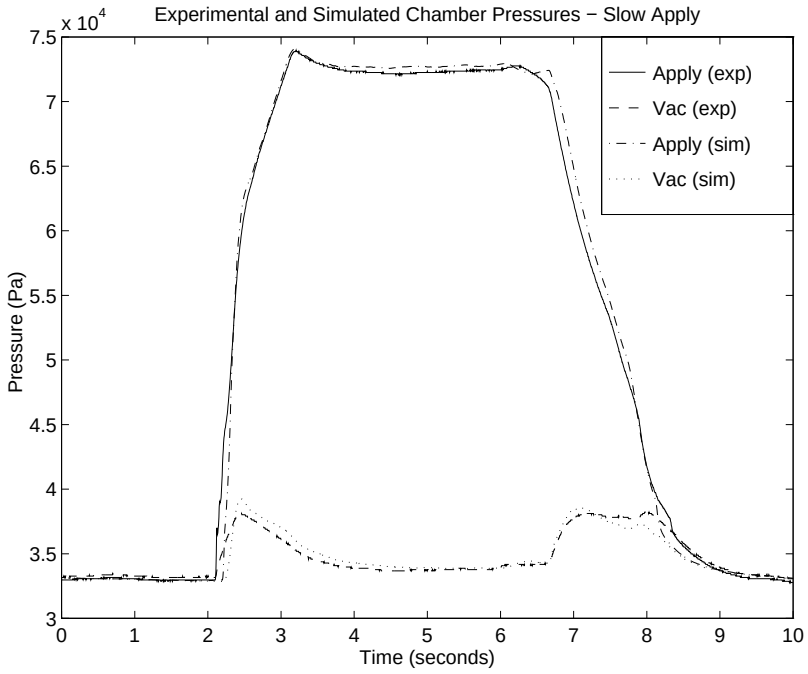

Figure 2.14: Chamber Pressures for Slow Apply

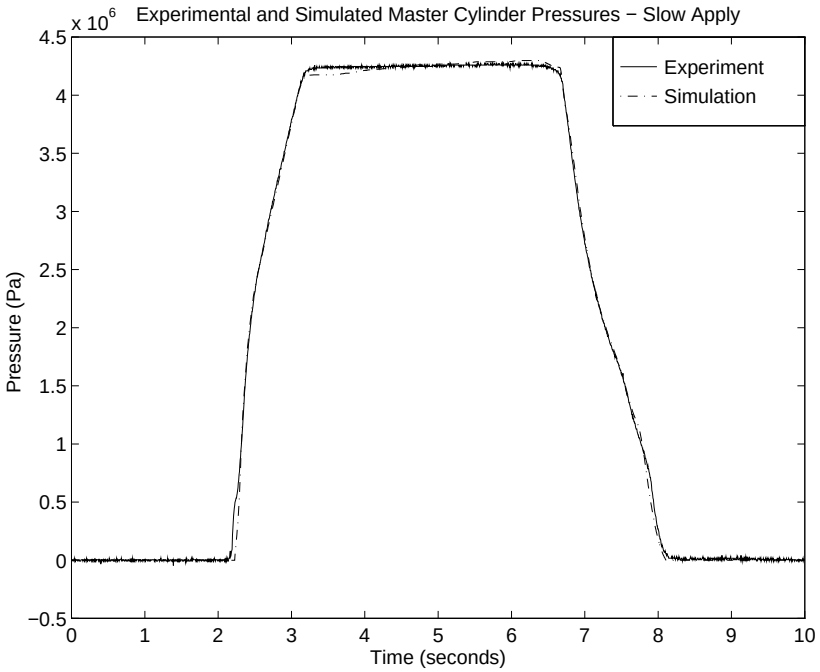

Figure 2.15: Master Cylinder Pressure for Slow Apply

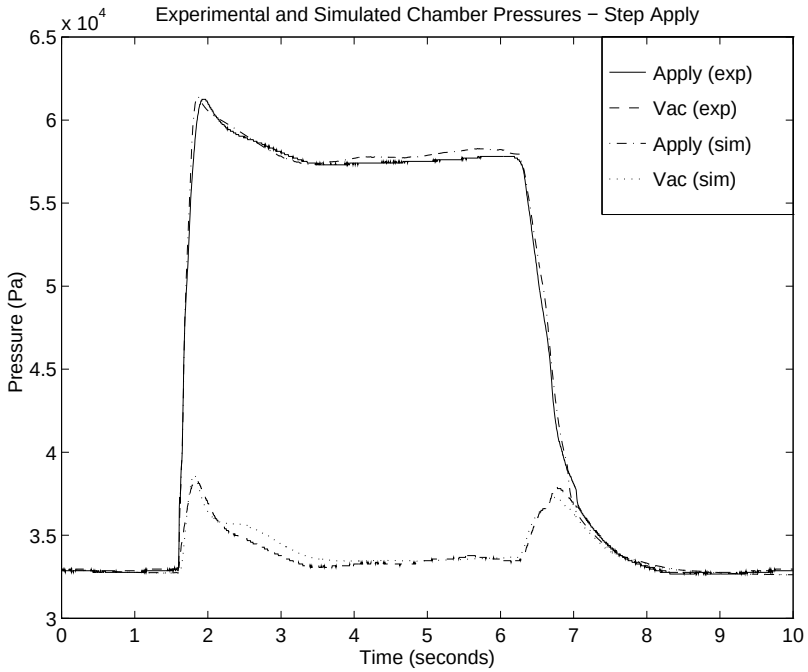

Figure 2.16: Chamber Pressures for Step Apply

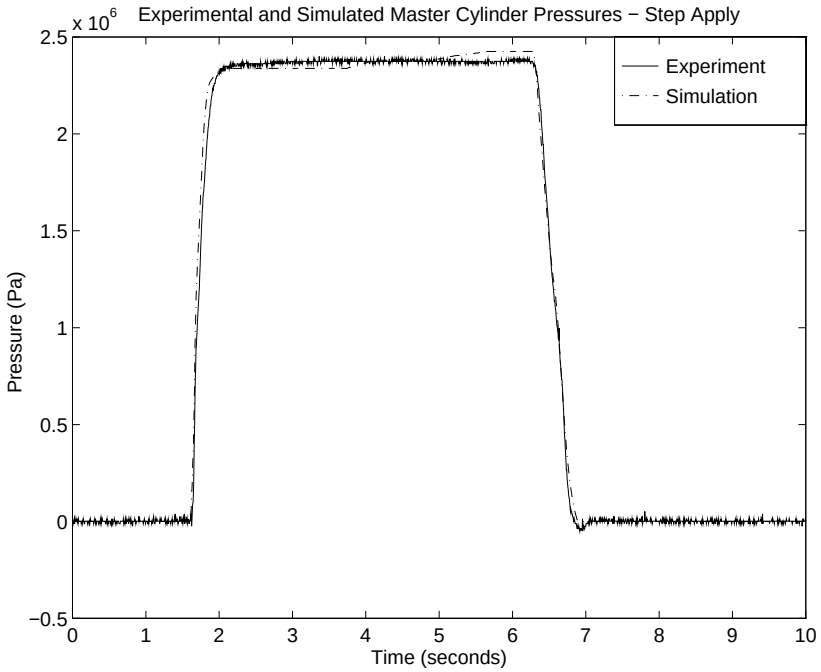

Figure 2.17: Master Cylinder Pressure for Step Apply

The fact that the simulations hold for a slow application underscores the success of the static control valve model in predicting the steady-state input-output relationship of the booster. In contrast, the accuracy shown in the step response provides a large measure of justification for the linearization used in the air flow equations. Indeed, the results produced exhibit greater accuracy than that demonstrated to date in the literature (Gerdes *et al.*, 1993; Khan *et al.*, 1994), even though more severe inputs were incorporated in this study. The model, therefore, exhibits sufficient fidelity for a simulation tool while retaining simplicity.

With any such work, the question of applicability to different vehicles naturally arises. The basic design of the booster, however, has changed little since the introduction of the reaction washer. As a result, boosters are a fairly standardized component and a survey of cut-away diagrams reveals little difference across passenger cars (*Motor Auto Repair Manual, Volumes 1 and 2*, 1991; *Motor Imported Car Repair Manual, Volumes 1 and 2*, 1991). Tandem boosters, with dual diaphragms, are visually quite different, but dynamically equivalent to the model presented here (Khan *et al.*, 1994). While specific flow coefficients, spring pre-loads and reaction washer characteristics determine the brake system "feel" and, hence, are subject to variation, such variation is captured by the general form of the model. In contrast, the hydraulic model is not exhaustive, but rather is intended to provide a basis for the analysis and design of AICC or platooning systems. Nevertheless, the development is general enough so that components (such as ABS) required by specific applications may be easily included.

2.3 Implications for Control

Because separate models were developed the individual brake system components, the control problems inherent in each of these components can be identified. As a result, an assessment of various brake actuation strategies for platooning can be made in terms of the prospects for control. Clearly, an actuator pulling on the brake pedal is by far the most straightforward design for applying the brakes. Such a strategy, however, incorporates all of the dynamics described in this chapter into the feedback loop. At the other extreme, actuating downstream of the booster (by creating an alternate

means of supplying force to the master cylinder or developing a traction control system with sufficiently high performance for platooning) reduces the dynamics in the feedback loop at the price of extensive redesign. The choice of actuation strategy, therefore, hinges on the suitability of each design for use in a closed-loop system.

Several aspects of the vacuum booster are particularly detrimental from this standpoint. First, the finite cut-in characteristic results in a finite brake line pressure below which the booster will not equilibrate. This means that attempting to control pressures below this level requires rapid modulation of the booster input. Even with a very high bandwidth actuator on the pedal, such modulation produces a high level of jerk, resulting in a deterioration of passenger comfort (this point is further supported in simulation by (Gerdes and Hedrick, 1995)). Conversely, simply refraining from actuating the brakes until this threshold level of pressure is commanded produces large tracking errors (Gerdes and Hedrick, 1995). Above the cut-in pressure, the hysteresis results in similar difficulties. Furthermore, the combination of (relatively) fixed atmospheric and vacuum pressures with a maximum orifice size serves as a rate limit on the booster output force. As a result of these limitations, experiments with pedal actuation tended to produce either reasonable tracking (Maciuca *et al.*, 1994) or acceptable comfort, but not both simultaneously.

The prospect of controlling the brake hydraulics directly is much more appealing. The single-state hydraulic model is quite simple and, from the results in Figure 2.12, quite accurate. Aside from the design issue, the only problem inherent with the brake hydraulics is the brake filling characteristics. Because of the nature of the brake fluid capacity in Figure 2.10, a certain quantity of fluid must flow to the brakes before the pressure at the wheel begins to rise. This raises the spectre of time delays to initiate braking, which can be quite problematic from a control perspective (Gerdes and Hedrick, 1995). Since this delay is a function of the fluid displaced and not a "pure" time delay in any sense, lead compensation should be able to reduce this problem. Direct actuation of the brake hydraulics and the design of a controller with appropriate lead compensation are the subject of the following chapter.

This does not mean that vacuum booster dynamics have no place in the analysis of automated highways, however. Other applications of vehicle control, such as collision avoidance systems or Autonomous Intelligent

Cruise Control (AICC), have very different performance requirements than platooning and may well be able to incorporate the vacuum booster. Furthermore, for at least the immediate future, people will continue to actuate vehicle brakes through vacuum boosters. A thorough understanding of these dynamics is therefore necessary to understand the interactions between the human driver and the automatic control system.

Chapter 3

Brake Control Using Dynamic Surface Control

3.1 Introduction

Variable Structure Control or Sliding Mode Control uses a discontinuous control structure to guarantee perfect tracking for a class of systems. It is particularly attractive to use this method in the control of automotive subsystems since most of them are highly nonlinear. Most methods of robust nonlinear control employ a Lyapunov Synthesis approach where the controlled variable is chosen to make the time derivative of a Lyapunov function candidate negative definite. Another method of recent interest is Integrator Backstepping. Although an elegant method, it has the problem of an "explosion of terms". Swaroop, et.al. solved this problem by the use of low pass filters integrated in the design of a so called Dynamic Surface Control. This paper extends their theory for the case when nonsmooth control is used. The advantage of such a controller is reduced final tracking error.

3.2 Nonsmooth Dynamic Surface Control

Consider the following system:

$$\begin{aligned} \dot{x}_1 &= x_2 + f_1(x_1) + \Delta f_1(x_1) \\ \dot{x}_2 &= x_3 + f_2(x_1, x_2) + \Delta f_2(x_1, x_2) \end{aligned}$$

$$
\begin{aligned}
&\cdots \\
\dot{x}_{n-1} &= x_n + f_{n-1}(x_1, \ldots, x_{n-1}) + \Delta f_{n-1}(x_1) \\
\dot{x}_n &= u
\end{aligned}
$$

The following assumptions are made for analysis:

- $|\Delta f_i(x_1, \ldots, x_i)| \leq \rho_i(x_1, \ldots, x_i)$ where ρ_i is a C^1 function in its arguments. Furthermore, ρ_i is not required to be Lipshitz and Δf_i is not required to be smooth or Lipshitz.
- f_i is a C^1 function in its arguments.

3.2.1 Controller Development

Define the tracking error to be

$$S_1 := x_1 - x_{1,des}$$

Define z such that

$$\tau_2 \dot{z}_2 + z_2 = -f_1(x_1) - sgn(S_1)\rho_1 - K_1 S_1 + \dot{x}_{1,des} = x_{2,des}$$

Continuing this design i times

$$
\begin{aligned}
S_i &:= x_i - z_i \\
\tau_{i+1}\dot{z}_{i+1} + z_{i+1} &= -f_i(x_1, \ldots, x_i) - sgn(S_i)\rho_i - K_i S_i + \dot{z}_i
\end{aligned}
$$

And the derivative of the tracking error is

$$\dot{S}_i = S_{i+1} + y_{i+1} - K_i S_i - sgn(S_i)\rho_i + \Delta f_i$$

Finally

$$
\begin{aligned}
S_n &= x_n - z_n \\
u_n &= \dot{z}_n - K_n S_n
\end{aligned}
$$

3.2.2 Background Theory

Definition 1 (Clarke's Generalized Gradient) *For a locally Lipshitz function $V : \Re^n \times \Re \to \Re$ define the generalized gradient of V at (x,t) by*

$$\partial V(x,t) = \overline{co}\left\{\lim \nabla V(x,t) | (x_i,t_i) \to (x,t), (x_i,t_i) \notin \Omega_V\right\}$$

where Ω_V is the set of measure zero where the gradient of V is not defined.

One way to view the generalized gradient at a point x is a set valued map equal to the convex closure of the limiting gradients near x. Two examples illustrate this idea.

Example 1 (Generalized Gradient 1) *$V(x) = |x|$ has a generalized gradient which equals*

$$\partial V(x) = \begin{cases} \{-1\} & x \in \Re^- \\ \{+1\} & x \in \Re^+ \\ [-1,+1] & x = 0 \end{cases}$$

Theorem 1 (Calculus for K) *The map K has the following properties*

1. *For $f : \Re^m \to \Re^n, \exists N_f \subset \Re^m, \mu N_f = 0$ s.t. $\forall N \subset \Re^m, \mu N = 0$,*

$$\bar{K}[f](x) = \overline{co}\left\{\lim f(x_i) | x_i \to x, x_i \notin N\right\}$$

2. *If f is continuous then*

$$\bar{K}[f](x) = \{f(x)\}$$

Definition 2 (Filippov) *A vector function $x(\cdot)$ is called a solution of $\dot{x} = f(x,t)$ on $[t_0,t_1]$ if $x(\cdot)$ is absolutely continuous on $[t_0,t_1]$ and for almost all $t \in [t_0,t_1]$*

$$\dot{x} \overset{a.e.}{\in} \bar{K}[f](x,t)$$

where

$$\bar{K}[f](x,t) := \bigcap_{\delta>0} \bigcap_{\mu N=0} \overline{co} f\left(B(x,\delta) \backslash N, t\right)$$

and $\bigcap_{\mu N=0}$ denotes the intersection over all all sets N of Lebesge measure zero.

Theorem 2 (Chain rule) *Let $x(\cdot)$ be a Filippov solution to $\dot{x} = f(x,t)$ on an interval containing t. Then $\dot{V}(x(t),t)$ exists almost everywhere and*

$$\frac{d}{dt}V(x(t),t) \in \dot{\tilde{V}}(x,t)$$

where

$$\dot{\tilde{V}}(x,t) := \bigcap_{\xi \in \partial V(x(t),t)} \xi^T \begin{pmatrix} \bar{K}[f](x(t),t) \\ 1 \end{pmatrix}$$

3.2.3 Stability Analysis

Swaroop proved the boundedness of tracking error using DSC. It is repeated here for completeness.

Theorem 3 (Tracking Error Boundedness for DSC) *Consider any non-Lipshitz nonlinear system in strict feedback form. Given any uncertain non-Lipschitz nonlinearity with a known C^1 function as its upper bound, and given any $p > 0$, $\epsilon > 0$, there exists a set of surface gains, $K_1, \ldots, K_n$ and time constants, $\tau_2, \ldots, \tau_n$ such that the Dynamic Surface Controller guarantees that if the trajectory is bounded, $x_{1,des}^2 + \dot{x}_{1,des}^2 + \ddot{x}_{1,des}^2 \leq K_0$, then the state of the system is regulated within a ball of radius $R(p, K_0)$, for all initial conditions in a ball of radius p, i.e. the closed loop system achieves semiglobal stable tracking.*

Proof: Define boundary layer error to be

$$\begin{aligned} y_{i+1} &= z_{i+1} + f_i(x_1, \ldots, x_i) + sgn(S_i)\rho_i + \frac{y_i}{\tau_i} + K_i S_i, \quad i \geq 2 \\ y_2 &= z_2 - x_{2,des} = z_2 + f_1(x_1) + sgn(S_1)\rho_1 + K_1 S_1 - \dot{x}_{1,des} \end{aligned}$$

whose derivative is

$$\dot{y}_2 = -\frac{y_2}{\tau_2} + \frac{\partial f_1}{\partial x_1}\dot{x}_1 + \frac{\partial sgn(S_1)}{\partial t}\rho_1 + sgn(S_1)\frac{\partial \rho_1}{\partial x_1}\dot{x}_1 + K_1\dot{S}_1 - \ddot{x}_{1,des}$$

Since $S_I := x_i - x_{i,des}$, it follows that

$$\begin{aligned} x_1 &= S_1 + x_{1,des} \\ x_2 &= S_2 + y_2 - f_1(x_1) - sgn(S_1)\rho_1 - K_1 S_1 + \dot{x}_{1,des} \\ x_{i+1} &= S_{i+1} + y_{i+1} - f_i(x_1, \ldots, x_i) - sgn(S_i)\rho_i(x_1, \ldots, x_i) - \frac{y_i}{\tau_i} - K_i S_i \end{aligned}$$

By induction,

$$x_{i+1} = \psi(S_1, \ldots, S_{i+1}, y_2, \ldots, y_{i+1}, K_1, \ldots, K_i, \tau_2, \ldots, \tau_i, x_{1,des}, \dot{x}_{1,des})$$

$$\begin{aligned} \dot{S}_i &= x_{i+1} + f_i(x_1, \ldots, x_i) + \Delta f_i(x_1, \ldots, x_i) - \dot{x}_{i,des} \\ &= S_{i+1} + y_{i+1} - K_i S_i - sgn(S_i)\rho_i(x_1, \ldots, x_i) + \Delta f_i(x_1, \ldots, x_i) \\ |\dot{S}_i| &\leq \Theta_i(S_1, \ldots, S_{i+1}, y_2, \ldots, y_{i+1}, K_1, \ldots, K_i, \tau_2, \ldots, \tau_i, x_{1,des}, \dot{x}_{1,des}) \end{aligned}$$

Similarly, it can be shown that

$$\begin{aligned} \frac{d\rho_i}{dt} &= \sum_1^i \frac{\partial \rho_i}{\partial x_j}\dot{x}_j \\ \left|\frac{d\rho_i}{dt}\right| &\leq \Theta_i(S_1, \ldots, S_{i+1}, y_2, \ldots, y_{i+1}, K_1, \ldots, K_i, \tau_2, \ldots, \tau_i, x_{1,des}, \dot{x}_{1,des}) \end{aligned}$$

The time derivative of y_{i+1} is

$$\dot{y}_{i+1} = -\frac{y_{i+1}}{\tau_{i+1}} + \sum_{j=1}^{i} \frac{\partial f_i}{\partial x_j}\dot{x}_j + \bar{K}\left[\frac{\partial sgn(S_i)}{\partial S_i}\right]\dot{S}_i\rho_i + \bar{K}[sgn(S_i)]\sum_{j=1}^{i}\frac{\partial \rho_i}{\partial x_j}\dot{x}_j + K_i\dot{S}_i + \frac{\dot{y}_i}{\tau_i}$$

By induction,

$$\left|\dot{y}_{i+1} + \frac{y_{i+1}}{\tau_{i+1}}\right| \leq \eta_{i+1}(S_1, \ldots, S_{i+1}, y_2, \ldots, y_{i+1}, K_1, \ldots, K_i, \tau_2, \ldots, \tau_i, x_{1,des}, \dot{x}_{1,des}, \ddot{x}_{i+1})$$

We also have

$$\dot{S}_i = S_{i+1} + y_{i+1} - K_i S_i - sgn(S_i)\rho_i + \Delta f_i$$

Define

$$V_{is} := \frac{S_i^2}{2}$$

and

$$V_{iy} := \frac{y_i^2}{2}$$

Then the respective derivatives are

$$\begin{aligned}\dot{V}_{is} &= S_i\left(S_{i+1} + y_{i+1} - K_i S_i - sgn(S_i)\rho_i + \Delta f_i\right) \\ &\leq |S_i|(|S_{i+1}| + |y_{i+1}| + |\Delta f_i|) - K_i S_i - |S_i|\rho_i \\ &\leq |S_i|(|S_{i+1}| + |y_{i+1}|) - K_i S_i\end{aligned}$$

and

$$\begin{aligned}\dot{V}_{iy} &= y_{i+1}\dot{y}_{i+1} \\ &\leq -\frac{y_{i+1}^2}{\tau_{i+1}} + |y_{i+1}|\eta_{i+1}(S_1, \ldots, S_{i+1}, y_2, \ldots, y_{i+1}, K_1, \ldots, K_i, \tau_2, \ldots, \tau_i, x_{1,des}, \dot{x}_{1,des}, \ddot{x}_{i+1})\end{aligned}$$

Pick a Lyapunov function candidate

$$V := V_{1s} + \ldots + V_{ns} + V_{2y} + \ldots + V_{ny}$$

For the system at hand,

$$x := [S_1 \ \ldots \ S_n \ y_2 \ \ldots \ y_n]^T$$

Therefore

$$\dot{\tilde{V}} = \nabla V^T \bar{K}[\dot{x}] \subset$$

$$\begin{bmatrix} \frac{\partial V}{\partial S_1} \\ \vdots \\ \frac{\partial V}{\partial S_n} \\ \frac{\partial V}{\partial y_2} \\ \vdots \\ \frac{\partial V}{\partial y_n} \end{bmatrix}^T \begin{bmatrix} \dot{S}_1 \\ \vdots \\ \dot{S}_n \\ \dot{y}_2 \\ \vdots \\ \dot{y}_n \end{bmatrix} =$$

$$\begin{bmatrix} S_1 \\ \vdots \\ S_n \\ y_2 \\ \vdots \\ y_n \end{bmatrix}^T \begin{bmatrix} S_2 + y_2 - \bar{K}[sgn(S_1)]\rho_1 - K_1 S_1 + \Delta f_1 \\ \vdots \\ -K_n S_n \\ -\frac{y_2}{\tau_2} + \frac{\partial f_1}{\partial x_1}\dot{x}_1 + \bar{K}\left[\frac{\partial sgn(S_1)}{\partial S_1}\right]\dot{S}_1\rho_1 + \bar{K}[sgn(S_1)]\frac{\partial \rho_1}{\partial x_1}\dot{x}_1 + K_1\dot{S}_1 - \ddot{x}_{1,des} \\ \vdots \\ -\frac{y_n}{\tau_n} + \sum_{j=1}^{n-1}\frac{\partial f_{n-1}}{\partial x_j}\dot{x}_j + \bar{K}\left[\frac{\partial sgn(S_{n-1})}{\partial S_{n-1}}\right]\dot{S}_{n-1}\rho_{n-1} + \bar{K}[sgn(S_{n-1})]\sum_{j=1}^{n-1}\frac{\partial \rho_{n-1}}{\partial x_j}\dot{x}_j + K_{n-1}\dot{S}_{n-1} + \end{bmatrix}$$

where

$$\bar{K}[sgn(S_i)] = SGN(S_i) = \begin{cases} -1 & S_i < 0 \\ [-1,+1] & S_i = 0 \\ +1 & S_i > 0 \end{cases}$$

and

$$\bar{K}\left[\frac{\partial sgn(S_i)}{\partial S_i}\right]\dot{S}_i\rho_i = 0$$

Therefore

$$\begin{aligned} S_i\dot{S}_i &= S_i\left(S_{i+1} + y_{i+1} - K_iS_i - SGN(S_i)\rho_i + \Delta f_i\right) \\ &\leq |S_i|\left(|S_{i+1}| + |y_{i+1}|\right) - K_iS_i^2 \\ y_i\dot{y}_i &= -\frac{y_i^2}{\tau_i} + y_i\left(\frac{\partial f_{i-1}}{\partial x_{i-1}}\dot{x}_{i-1} + SGN(S_{i-1})\frac{\partial \rho_{i-1}}{\partial x_{i-1}}\dot{x}_{i-1} + K_{i-1}\dot{S}_{i-1} + \frac{\dot{y}_{i-1}}{\tau_{i-1}}\right) \\ &\leq -\frac{y_i^2}{\tau_i} + |y_i|\eta_i(S_1,\ldots,S_i,y_2,\ldots,y_i,K_1,\ldots,K_{i-1},\tau_2,\ldots,\tau_{i-1},x_{1,des},\dot{x}_{1,des},\ddot{x}_{1,des}) \end{aligned}$$

Above $SGN(S_i)$, $\dot{S}_{i-1}$ and $\dot{x}_i$ are bounded and $\frac{\partial f_i}{\partial x_i}$ and $\frac{\partial \rho_i}{\partial x_i}$ are continuous, therefore a continuous function η_i can be found.

Claim 1 *Given any $p > 0$,K_0, s.t. $\forall V(0) \leq p$, and $|x_{1,des}|^2 + |\dot{x}_{1,des}|^2 + |\ddot{x}_{1,des}|^2 \leq K_0$, there exists a set of gains, $K_1,\ldots,K_n$, and filter time constants, $\tau_2,\ldots,\tau_n$, s.t. $V(t) \leq p\,\forall t > 0$ and $\dot{V} \leq -2\alpha_0 V + n\left(\frac{\epsilon}{2}\right)$*

Proof 1 (Claim) *Choose the following set of gains:*

$$\begin{aligned} K_i &= 2 + \alpha_0 \\ \frac{1}{\tau_{i+1}} &= 1 + \frac{M_{i+1}^2}{2\epsilon} + \alpha_0 \end{aligned}$$

Therefore

$$\begin{aligned} \dot{V} &= \sum_1^n -(2+\alpha_0)S_i^2 + \frac{2S_i^2 + S_{i+1}^2 + y_{i+1}^2}{2} \\ &\quad + \sum_1^{n-1} -\left(1 + \frac{M_{i+1}^2}{2\epsilon} + \alpha_0\right)y_{i+1}^2 + \frac{M_{i+1}^2 y_{i+1}^2}{2\epsilon}\frac{\eta_{i+1}^2}{M_{i+1}^2} + \frac{\epsilon}{2} \\ &\leq -2\alpha_0 V + n\left(\frac{\epsilon}{2}\right) - \left(1 - \frac{\eta_{i+1}^2}{M_{i+1}^2}\right)\frac{M_{i+1}^2 y_{i+1}^2}{2\epsilon} \end{aligned}$$

On $V(S_1, \ldots, S_n, Y_2, \ldots, y_n) = p$, $\eta_{i+1} \leq M_{i+1}$. Therefore,

$$\dot{V} \leq -2\alpha_0 p + n\epsilon$$

Eventually tracking error resides in a ball of radius $\frac{n\left(\frac{\epsilon}{2}\right)}{2\alpha_0} < \frac{n\epsilon}{2\alpha_0}$.

Chapter 4

Adpative Control

4.1 Brake Torque Coefficient Adaptation

Although there is a quasi-linear relationship between slave cylinder pressure and brake torque, that relationship varies with several parameters including, but not limited to, temperature, friction material and speed. Under these conditions, robustness can be achieved through the use of adaptive control algorithms. Lyapunov-based adaptive control algorithms were developed to compensate for the variation in friction coefficient between the brake rotors and brake pads. A thorough investigation of the available systems of direct brake torque measurement was performed. The winning solution is an instrumented brake rotor. The rotor deflection is measured using a set of strain gages. The measurement is then transmitted to the computer via a transmitter/receiver pair.

This section develops a control algorith that uses an estimate of the coefficient between brake pressure and brake torque. For velocity following define

$$\varepsilon := v_{lead} - v$$

Define the sliding surface as

$$S := c_1\dot{\varepsilon} + c_2\varepsilon$$

whose derivative is

$$\dot{S} = c_1\ddot{\varepsilon} + c_2\dot{\varepsilon}$$

where $\ddot{\varepsilon} = a - a_{lead}$

The acceleration is related to the longitudinal forces by

$$a = \frac{(T_e - Crv^2 - rR - P_{w,des}K)}{\beta}$$

where

$$\begin{aligned} T_e &= minimum\ engine\ torque \\ Crv^2 &= aerodynamic\ drag \\ rR &= rolling\ resistance \\ P_w &= brake\ torque \end{aligned}$$

We want $\dot{S} = -\lambda S$ therefore

$$\dot{S} = c_1 \left(\frac{T_e - Crv^2 - rR - P_{w,des}K}{\beta} - a_{lead} \right) + c_2 \dot{\varepsilon} = -\lambda S \tag{4.1}$$

from which the desired input, based on the estimate of K is obtained:

$$P_{w,des} = \frac{T_e - Crv^2 - rR + \beta \left(\frac{c_2 \dot{\varepsilon} + \lambda S}{c_1} - a_{lead} \right)}{\hat{K}} \tag{4.2}$$

Plugging Equation 4.2 into 4.1 and adding and subtracting λS, $\dot{S}$ can be rewritten as:

$$\dot{S} = \frac{c_1}{\beta \hat{K}} \tilde{K} \left(T_e - Crv^2 - rR - \beta a_{lead} \right) + \frac{\tilde{K}}{\hat{K}} \left(c_2 \dot{\varepsilon} + \lambda S \right) - \lambda S \tag{4.3}$$

where $\tilde{K} = \hat{K} - K$

Define a Lyapunov function candidate

$$V := \frac{S^2}{2} + \frac{\tilde{K}^2}{2\gamma} \tag{4.4}$$

whose derivative is

$$\dot{V} = S\dot{S} + \frac{\tilde{K}\dot{\hat{K}}}{\gamma} \tag{4.5}$$

Plug Equation 4.3 into 4.5 to obtain

$$\dot{V} = \frac{\tilde{K}}{\hat{K}} \left(\frac{c_1}{\beta} \left(T_e - Crv^2 - rR - \beta a_{lead} \right) + c_2 \dot{\varepsilon} + \lambda S \right) S - \lambda S^2 + \frac{\tilde{K}\dot{\hat{K}}}{\gamma} \tag{4.6}$$

For future simplicty define

$$\mathcal{A} = \frac{c_1}{\beta}\left(T_e - Crv^2 - rR - \beta a_{lead}\right) + c_2\dot{\varepsilon} + \lambda S$$

For stability we need $\dot{V} = -\lambda S$, therefore

$$\dot{\hat{K}} = -\gamma\frac{\mathcal{A}S}{\hat{K}} \tag{4.7}$$

Having $\dot{V} = -\lambda S$ implies that $V(t) \leq V(0)$ therefore S and $\tilde{K}$ are bounded. The invariant set theorem cannot be used to conclude the convergence of $\tilde{K}$ because the dynamics are nonautonomous. Therefore Barbalat's Lemma will be used to check the uniform continuity of $\dot{V}$

$$\ddot{V} = -2\lambda S\dot{S} \tag{4.8}$$

Since S and $\tilde{K}$ are bounded as shown above and everything else in $\dot{S}$ is bounded implies that $\dot{V}$ is uniformly continuous. Application of Barbalat's Lemma the shows that $S \to 0$ as $t \to \infty$.

4.2 Non-smooth Lyapunov Function

If the Lyapunov function candidate is instead defined as

$$V := Ssgn(S) + \frac{\tilde{K}^2}{2\gamma} \tag{4.9}$$

with the time derivative

$$\dot{V} := \dot{S}sgn(S) + \frac{\tilde{K}\dot{\hat{K}}}{\gamma} \tag{4.10}$$

Therefore

$$\dot{\hat{K}} = -\gamma\frac{\mathcal{A}sgn(S)}{\hat{K}} \tag{4.11}$$

However, since $sgn(S)$ is undefined at $S = 0$, $\dot{V}$ is also undefined at $S = 0$.

For the current system

$$x = \begin{bmatrix}\hat{K} & S\end{bmatrix}^T \tag{4.12}$$

As defined in the chain rule

$$\dot{\tilde{V}} = \nabla V^T \bar{K}[\dot{x}] \subset$$
$$\begin{bmatrix} \frac{\tilde{K}}{\gamma} \\ \frac{\partial V}{\partial S} \end{bmatrix}^T \begin{bmatrix} -\frac{\gamma}{\tilde{K}} \mathcal{A} \bar{K}\left[sgn(S)\right] \\ \frac{\tilde{K}}{\tilde{K}} \mathcal{A} - \lambda S \end{bmatrix} \tag{4.13}$$

In this particular case

$$\frac{\partial V}{\partial S} = \bar{K}\left[sgn(S)\right] = SGN(S) = \begin{cases} \{-1\} & S < 0 \\ [-1, +1] & S = 0 \\ \{+1\} & S > 0 \end{cases} \tag{4.14}$$

Evaluating Equation 4.13

$$\dot{\tilde{V}} = -\lambda S \cdot SGN(S) \tag{4.15}$$

Therefore $\dot{\tilde{V}} \leq 0$ which, according to Shevitz and Paden (1993), guarantees that $V(t) \leq V(0)$. Therefore S and $\hat{K}$ are bounded.

In order to apply Barbalat's Lemma, $\ddot{V}$ needs to be obtained

$$\ddot{V} = \nabla \dot{V}^T \bar{K}[\dot{S}] \tag{4.16}$$

which evaluates to

$$\ddot{V} = \begin{cases} -\lambda \dot{S} & S > 0 \\ \lambda \dot{S}\left[-1, +1\right] & S = 0 \\ \lambda \dot{S} & S < 0 \end{cases} \tag{4.17}$$

which is bounded since $\dot{S}$ is bounded and therefore $\dot{V}$ is uniformly continuous. According to Barbalat's Lemma this implies that $S \to 0$.

The experimental setup mentioned at the begining of this chapter will be used to validate the quality of this controller.

Chapter 5

Coordinated Throttle and Brake Control

Having treated brake modeling and controller design in the previous two chapters, we now turn attention towards applying these results to the vehicle control problem. Specifically, we seek a controller structure which can modulate the engine and brake torques as necessary to perform the four basic longitudinal control actions of speed control, spacing control, platoon joining and platoon splitting. This chapter approaches the design of such a structure from the standpoint of multiple-surface sliding control, in the spirit of previous work by (McMahon *et al.*, 1990) and others. The resulting controller consists of three elements: an "upper" surface controller dependent upon the longitudinal control task, a switching logic to choose between brake and throttle control and separate "lower" surface controllers for engine and brake torques. Under the formalism of multiple-surface sliding control, the upper surface controller is designed by assuming that the longitudinal vehicle acceleration may be controlled directly. Tracking this acceleration, which is designated a "synthetic input," subsequently becomes the control objective for the lower surface controllers. Intuitively, if the engine and brake dynamics are fast, relative to the desired acceleration, such decoupling of the design problem produces acceptable performance.

As described later, both the multiple-surface controller and the switching condition can be put into a broader mathematical framework. Within this framework, very rigorous guarantees of system performance can be derived and issues of gain selection and saturation treated explicitly. The

true strengths of these mathematics, however, are the extent to which they can be applied to real systems with nonlinearities, uncertainties and neglected actuator dynamics and the intuitive design procedure that results. Accordingly, this chapter presents a physically intuitive approach to the problem of vehicle control. Section 5.4 presents a switching logic for coordinating the throttle and brake controllers and a means of determining the desired brake and engine torques. In order to reduce potential chatter across the interface in implementation, a hysteresis element is added to this logic. The chapter concludes with simulation results validating the use of the coordinated control structure within the context of speed and spacing control.

5.1 Vehicle Modeling

5.1.1 Longitudinal Vehicle Model

Figure 5.1 shows the free-body diagrams for the chassis, driving and driven wheels of a typical (rear-wheel drive) passenger car encountering a grade with angle θ. Balancing the forces on the chassis in the longitudinal direction gives:

$$R_{af} + R_{ar} - F_a - m_c g \sin\theta = m_c a \tag{5.1}$$

where R_{af} and R_{ar} are the reaction forces at the front and rear axles, respectively, F_a is the aerodynamic drag force and m_c is the mass of the chassis. Each wheel provides two additional equations. For the driving (rear) wheel:

$$\tau_d - hF_{trr} - M_{rrr} - \tau_{br} = \bar{J}_{wr}\alpha_{wr} \tag{5.2}$$

$$-R_{ar} + F_{trr} - m_{wr} g \sin\theta = m_{wr} a \tag{5.3}$$

and for the driven wheel:

$$-hF_{trf} - M_{rrf} - \tau_{bf} = J_{wf}\alpha_{wf} \tag{5.4}$$

$$-R_{af} + F_{trf} - m_{wf} g \sin\theta = m_{wf} a \tag{5.5}$$

In these equations, τ_d is the engine drive torque referred to the axle, F_{trr} and F_{trf} are the tractive forces at the rear and front wheels, respectively, M_{rrr}

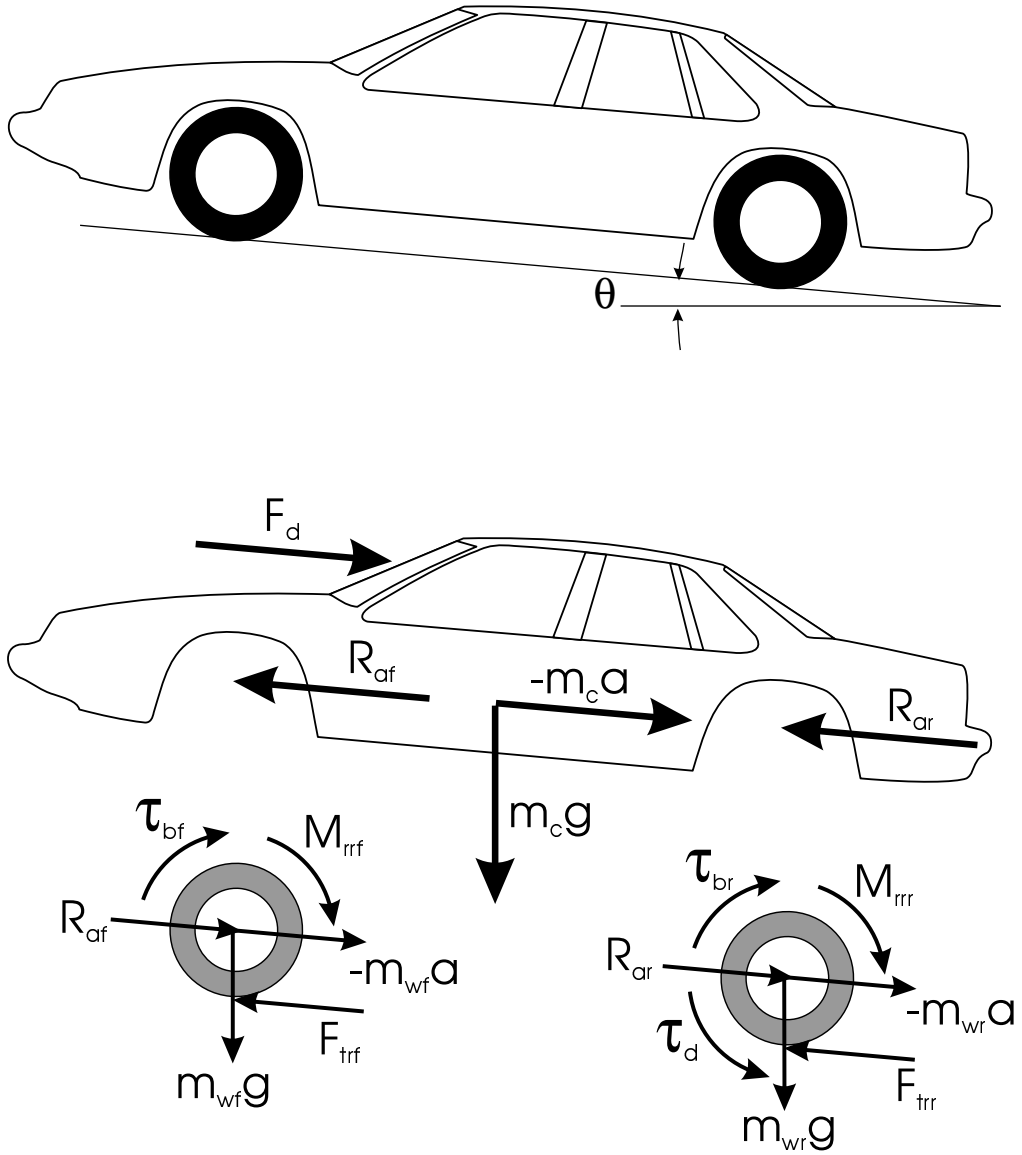

Figure 5.1: Free Body Diagram for Longitudinal Motion of Automobile

and M_{rrf} denote the rolling resistance moments, τ_{br} and τ_{bf} are the brake torques and h is the effective wheel radius. m_{wr} and m_{wf} are the wheel (axle) masses, α_{wr} and α_{wf} are the angular accelerations of the wheels, J_{wf} is the front axle inertia and $\bar{J}_{wr}$ represents the effective inertia of the rear axle, transmission and engine, referred to the rear axle.

Combining Equations 5.1, 5.3 and 5.5 gives a single equation for the longitudinal motion of the vehicle:

$$F_{trr} + F_{trf} - F_a - mg\sin\theta = ma \tag{5.6}$$

where m is the total curb weight of the vehicle (*i.e.* $m = m_c + m_{wf} + m_{wr}$). Unfortunately, this equation is in terms of the tractive forces instead of the engine and brake torques, which are considered to be the controls. Substituting the expressions for the tractive forces in Equations 5.2 and 5.4, however, yields:

$$\left[\tau_d - \tau_{br} - \tau_{bf} - M_{rrr} - M_{rrf} - \bar{J}_{wr}\alpha_{wr} - J_{wf}\alpha_{wf}\right]/h - F_a - mg\sin\theta = ma \tag{5.7}$$

At this point, we make the first simplifying assumption that no slip occurs at the wheels. Strictly speaking, this is not true, since the development of a tractive force implies some deformation of the contact patch of the tire and, consequently, some slip. At the low levels of acceleration considered in this work for general automated highway maneuvers, however, slip is quite small and the tire dynamics may safely be neglected. This no slip assumption has been incorporated in previous designs for longitudinal control (McMahon *et al.*, 1992; Hedrick *et al.*, 1993) and the validity confirmed experimentally (McMahon *et al.*, 1992). It should be stressed, however, that the development here is tied to situations where this assumption is valid. Consequently, the resulting control law is not applicable to scenarios which involve considerable tire slip, such as emergency braking. Using this assumption,

$$\alpha_{wr} = \alpha_{wf} = a/h \tag{5.8}$$

and the longitudinal equation reduces to:

$$\left[\tau_d - \tau_b - M_{rr}\right]/h - F_a - mg\sin\theta = \left(m + \left(\bar{J}_{wr} + J_{wf}\right)/h^2\right)a \tag{5.9}$$

where $M_{rr} = M_{rrr} + M_{rrf}$ and $\tau_b = \tau_{br} + \tau_{bf}$. Note that this assumption implies that the distribution of rolling resistance or braking force on the axles is not important; the sum is the only quantity involved.

The final step is to relate the drive torque on the axle, τ_d, to the net torque produced by the engine, τ_e. This requires some representation of the transmission including, for cars with an automatic transmission, the torque converter. Normally, the torque converter produces some slip between the engine and axle, necessitating the introduction of additional states (McMahon *et al.*, 1990). Here, however, we assume that the torque converter is locked (as in (Hedrick *et al.*, 1991)) so that the engine speed, ω_e, and vehicle speed, v, may be directly related through the gear ratio, R_g:

$$v = R_g \; h \; \omega_e \tag{5.10}$$

Similarly, for the accelerations,

$$a = R_g \; h \; \dot{\omega}_e \tag{5.11}$$

In this context, the gear ratio, R_g, represents the combination of the gearbox and final driveline reduction. For the experimental vehicles in question, the assumption of a locked torque converter is, in fact, strictly true in both 3rd and 4th gears and when locked in 1st, since a mechanical clutch is present in these configurations.

Using the gear ratio, the relation between τ_e and τ_d is simply:

$$\tau_e = R_g \tau_d \tag{5.12}$$

and the lumped inertia described by $\bar{J}_{wr}$ can be defined as:

$$\bar{J}_{wr} = J_{wr} + J_e / {R_g}^2 \tag{5.13}$$

where J_{wr} is the inertia of the rear axle and wheel and J_e is the inertia of the engine and transmission. Using Equations 5.9 and 5.11 through 5.13, the longitudinal equation may be written as:

$$\tau_e - R_g \left(\tau_b + M_{rr} + hF_a + mgh \sin\theta\right) = \frac{1}{R_g h} \left[J_e + {R_g}^2 \left(J_{wr} + J_{wf} + mh^2\right)\right] a \tag{5.14}$$

Defining

$$\beta = \left[J_e + {R_g}^2 \left(J_{wr} + J_{wf} + mh^2\right)\right] / (R_g h) \tag{5.15}$$

gives the final longitudinal equation

$$\tau_e - R_g \left(\tau_b + M_{rr} + hF_a + mgh \sin\theta\right) = \beta a \tag{5.16}$$

Under the assumptions above, Equation 5.16 forms the state equation for both the engine speed, ω_e, and the vehicle speed, v.

This equation also relates the vehicle acceleration to the grade and drag forces and the two controls, τ_e and τ_b. The dynamic equations for τ_b were developed in the previous chapter and those for τ_e are presented in the following section. For the drag forces, M_{rr} is taken as an experimentally determined constant (though there is known to be some slight speed dependence) and F_a has the form

$$F_a = C_a v^2 \tag{5.17}$$

where C_a is the aerodynamic drag coefficient. Equation 5.16 is the key to translating desired vehicle acceleration (determined from the vehicle control objective) into desired brake and engine torques and, as will be detailed later, forms the basis for the switching criterion.

5.1.2 Engine Modeling

The engine model used in this work is a simple two-state model based upon work by (Moskwa and Hedrick, 1987) and (Cho and Hedrick, 1989) and previously used for longitudinal control by several researchers (McMahon *et al.*, 1990; Hedrick *et al.*, 1991; McMahon *et al.*, 1992). In this model, the engine torque production is continuous and determined from a steady-state engine map

$$\tau_e = \tau_e \left(\omega_e, P_m\right) \tag{5.18}$$

where P_m is the pressure in the engine intake manifold. Figure 5.2 shows the steady-state map for one of the experimental vehicles. This map is based upon data provided by the Ford Motor Company, although to ensure a closer correlation between simulation and experimental results, the entries of the map corresponding to engine drag torques were modified. This modification was accomplished by measuring the manifold pressure, engine speed and deceleration during coast-down tests in first gear. The actual engine drag torque was determined from the vehicle deceleration, after subtracting the effects of aerodynamic drag and rolling resistance, and the engine map modified accordingly.

The two states are taken to be the engine speed, ω_e, and the mass of air in the intake manifold, m_a, which is related to manifold pressure, P_m, by

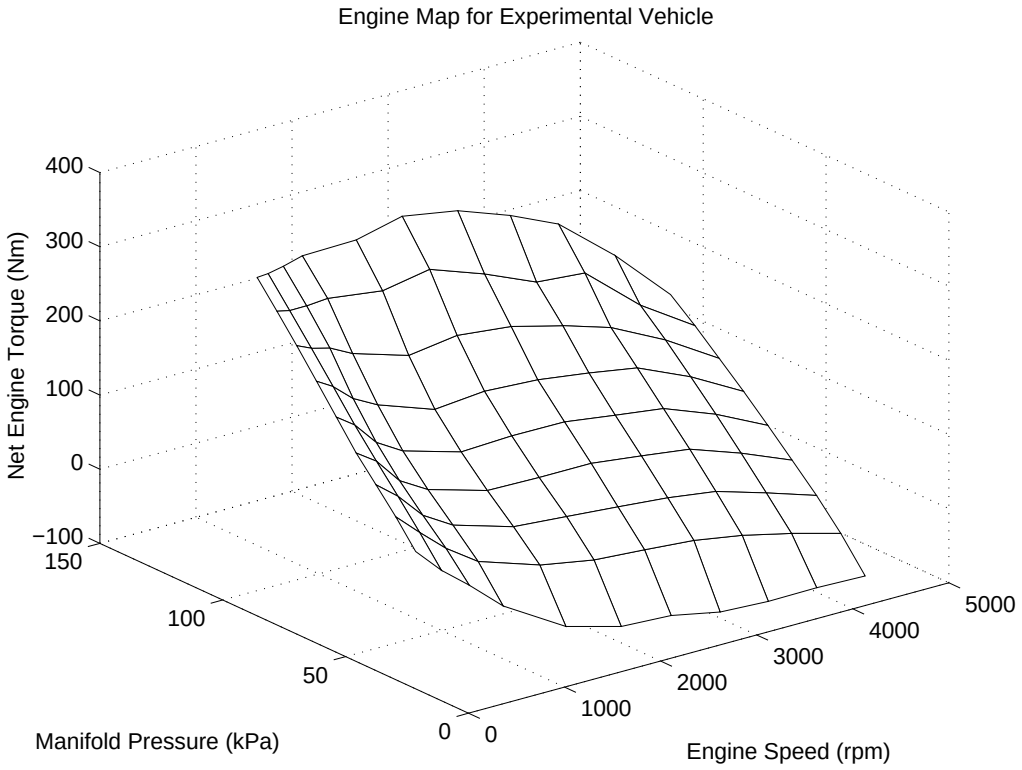

Figure 5.2: Engine Map for Experimental Vehicle

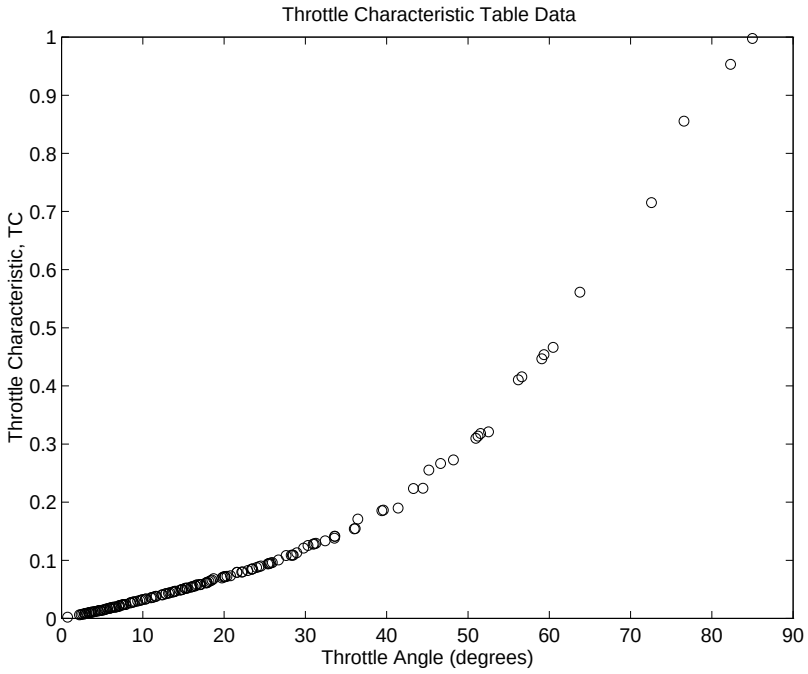

Figure 5.3: Throttle Characteristic

assuming ideal gas behavior:

$$P_m V_m = m_a R T_m \tag{5.19}$$

Hence the air mass and the manifold pressure may be used interchangeably. The state equation for ω_e is simply Equation 5.16, while the state equation for m_a is given by continuity:

$$\dot{m}_a = \dot{m}_{ai} - \dot{m}_{ao} \tag{5.20}$$

The mass of air flowing into the intake manifold is given by

$$\dot{m}_{ai} = \text{MAX TC}\,(\alpha)\,\text{PRI}\,(m_a) \tag{5.21}$$

where MAX represents the flow rate at full throttle, α is the throttle angle, TC(α) is an empirical throttle characteristic (obtained from a look-up table plotted in Figure 5.3) and PRI(m_a) a pressure influence function for

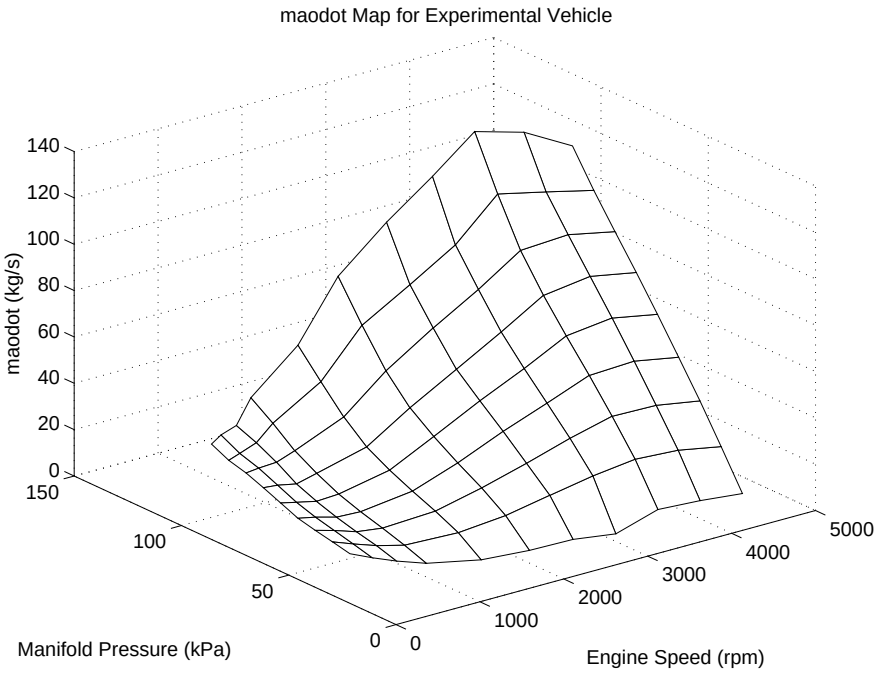

Figure 5.4: Empirical Map for $\dot{m}_{ao}$

compressible flow:

$$\text{PRI} = 1 - \exp\left(9 \cdot \left(\frac{P_m}{P_{atm}} - 1\right)\right) \tag{5.22}$$

The mass of air flowing out of the intake manifold and into the cylinders may be determined analytically by:

$$\dot{m}_{ao} = \frac{V_e}{4\pi V_m}\, \eta_{vol}\; m_a\; \omega_e \tag{5.23}$$

where V_e and V_m denote engine displacement and manifold volume, respectively, and $\eta_{vol}(\omega_e, m_a)$ is the volumetric efficiency of the engine. In practice, however, this value is obtained from an empirical map, $\dot{m}_{ao}(m_a, \omega_e)$, illustrated in Figure 5.4.

As indicated by Figure 5.3, the throttle characteristic is zero when the throttle is completely closed. Physically speaking, however, the air flow into the manifold cannot completely stop, since the engine continues to run. This

apparent contradiction results from the fact that the basic model does not include the throttle bypass, which lets air into the manifold when the throttle is closed. Since braking generally takes place at closed throttle, a model of this bypass behavior is extremely important for coordinating throttle and brake control.

Because the bypass in modern cars generally involves a proprietary control algorithm to regulate flow, the bypass model used here is empirical, rather than analytical. The data necessary for such a model were obtained as follows. First, a series of experimental tests was performed to determine the steady-state manifold pressure at closed throttle as a function of engine speed. This function was obtained by allowing the vehicle to coast in gear while measuring the manifold pressure and engine speed. Since the dynamics associated with the manifold air flow are much faster than those associated with the engine speed, these tests produced a good approximation of this steady-state behavior. Indeed, the results were consistent within measurement noise across different test runs and while the vehicle was locked in different gears (1st, 3rd and 4th gear were investigated).

From these tests, the steady-state manifold pressure can be plotted as a function of engine speed, as illustrated by Figure 5.5. Physically, this curve is also the projection of the lower edge of the engine map in Figure 5.2 into the plane determined by P_m and ω_e. Note that the noise in this plot is indicative of pressure transients in the manifold and not sensor noise (this was confirmed by measurements from two redundant sensors of different manufacture). The relationship in Figure 5.5 can be construed either as a limit on how low m_a can drop or as a constraint on $\dot{m}_a$. Under the latter interpretation, $\dot{m}_a$ is given by Equation 5.20 for points lying on or above the curve and modeled as a large positive constant for points below the curve (thereby forcing the state to remain on or above the curve). This approach is taken in the simulation, since numerically it is much easier to limit the state derivatives than the actual states.

5.2 Engine Controller Development

The engine controller incorporated into this design is a sliding control scheme based upon the two-state engine model in the previous section and previously used for highway automation by (McMahon *et al.*, 1990), (Hedrick *et al.*,

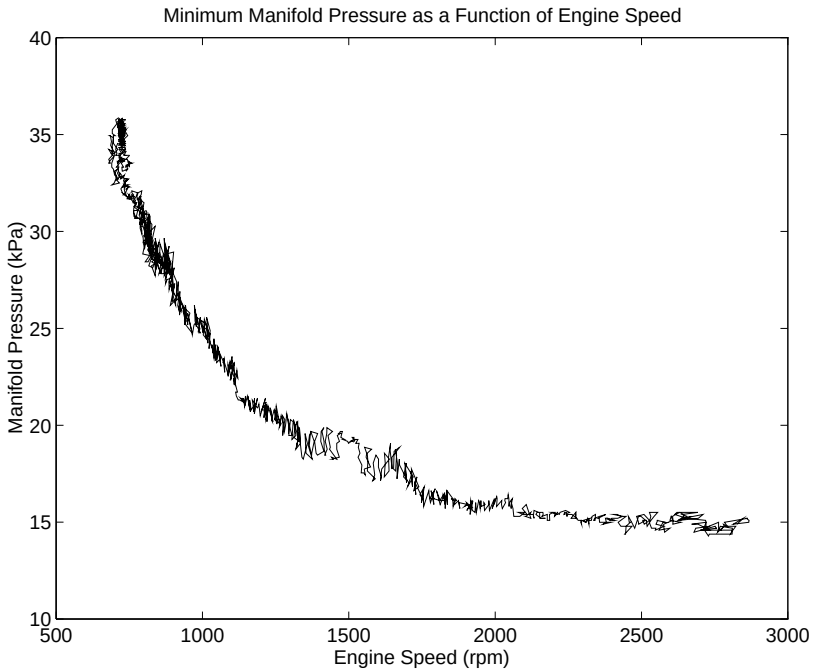

Figure 5.5: Manifold Pressure as a Function of Engine Speed from Coast Down

1991) and (McMahon *et al.*, 1992), among others. As originally derived, this controller does not include the bypass at closed-throttle. However, the modification of the engine model to include the bypass (as described in Section 5.1.2) has no effect on the controller design, except to define the limits of engine torque production. This limitation is accounted for by the switching logic in Section 5.4 and not the engine control algorithm.

The engine controller calculates the desired value of the throttle angle, α, so that the engine torque production, τ_e, tracks the desired value, τ_{edes}. Using the principle that the dynamics associated with the mass of air in the intake manifold (Equation 5.20) are much faster than those associated with the engine speed (Equation 5.16), τ_{edes} can be translated into a desired value of m_a at the current value of ω_e by solving Equation 5.18 implicitly:

$$\tau_{edes} = \tau_e \left(\omega_e, P_{mdes} \right) \tag{5.24}$$

and calculating m_{ades} from P_{mdes}. Defining the sliding surface for engine control, S_e:

$$S_e = m_a - m_{ades} \tag{5.25}$$

we set

$$\dot{S}_e = -\lambda_e S_e \tag{5.26}$$

Using Equations 5.20 through 5.23, the sliding surface equations yield a desired flow of air into the manifold:

$$\dot{m}_{ai} = \dot{m}_{ao} \left(m_a, \omega_e \right) + \dot{m}_{ades} - \lambda_e \left(m_a - m_{ades} \right) \tag{5.27}$$

From this, follows the desired throttle characteristic:

$$TC_{des} \left(\alpha \right) = \left(\dot{m}_{ao} + \dot{m}_{ades} - \lambda_e S_e \right) / \left(\text{MAX PRI} \right) \tag{5.28}$$

Inverting the throttle characteristic yields the value of the control, α.

5.3 Longitudinal Control Actions

With respect to longitudinal motion alone, there are four basic control actions: speed control, spacing control, platoon joining and platoon splitting. Under speed control, the vehicle acts either autonomously or as the lead car in a platoon, attempting to track a desired (generally time-dependent) velocity.

Spacing control is employed by the remaining cars in the platoon, which incorporate measurements of the distance and closing rate to the preceding vehicle (and potentially position, velocity and acceleration information from the lead and preceding vehicles) to maintain a desired spacing throughout maneuvers. In platoon joining, a platoon of vehicles closes the distance between itself and the preceding platoon in a manner that ensures safety. Conversely, in platoon splitting, a platoon of vehicles separates, with the trailing vehicles dropping back and beginning to function as an autonomous platoon.

While these four functions are fundamentally different, they share two common aspects. First, all of these functions can be - and have been - formulated as a sliding control problem, with the desired control task achieved when a particular sliding surface is forced to zero. Secondly, in this sliding control formulation, the desired vehicle acceleration is used as a synthetic input. Clearly, a nice modular structure can be achieved if the coordinated throttle and brake controller is designed to function with any of these control tasks. This, in turn, requires that the engine and brake control problems be cast in terms of tracking the synthetic input. This section discusses the development of control laws for the four basic longitudinal functions and presents the desired vehicle acceleration as a function of the relevant parameters. Section 5.4 details the switching logic and describes how the desired acceleration can be translated into throttle and brake commands.

5.3.1 Speed Control

Controller design for the speed control task is fairly trivial. Given a desired velocity, $v_{des}(t)$, define the sliding surface S_u by:

$$S_u = v - v_{des} \tag{5.29}$$

Because sliding control methods are also used for the throttle and brake controllers, S_u will be referred to often as the "upper" sliding surface or, simply, the upper surface. Clearly, our control objective is satisfied when $S_u = 0$. To achieve this, the system state is "driven" to this surface by defining:

$$\dot{S}_u = -\lambda_u S_u \tag{5.30}$$

Solving Equation 5.30 yields the desired vehicle acceleration (or synthetic input), a_{synth}:

$$a_{synth} = \dot{v}_{des} - \lambda_u (v - v_{des}) \tag{5.31}$$

5.3.2 Spacing Control

Several formulations spacing control or vehicle follower laws have appeared in the literature, each with different information requirements and performance characteristics (for a good discussion of various strategies, see (Swaroop, 1994)). Here, we discuss only one example, due to (Swaroop and Hedrick, 1994). Given a platoon of n vehicles, we designate the car in front as the lead vehicle and number the remaining vehicles as followers, beginning with the second car or first follower. The position, velocity and acceleration of the lead car are given by x_{lead}, $\dot{x}_{lead}$ and $\ddot{x}_{lead}$, respectively, and the corresponding quantities for the remaining cars are denoted by x_i, $\dot{x}_i$ and $\ddot{x}_i$, where $i = 1 \ldots (n-1)$. The controller derivation proceeds as follows.

Assuming constant desired spacing between vehicles, Δ, we define the spacing error for car i in terms of the position of cars i and $i-1$, x_i and x_{i-1}:

$$\epsilon_i = \Delta - (x_{i-1} - x_i) \tag{5.32}$$

For car 1, the previous vehicle is the platoon leader and Equation 5.32 becomes

$$\epsilon_1 = \Delta - (x_{lead} - x_1) \tag{5.33}$$

Assuming that lead vehicle information and the car length, L_i, are known, acceptable error dynamics form the first surface (Swaroop and Hedrick, 1994):

$$S_{ui} = \dot{\epsilon}_i + q_1 \epsilon_i + q_3(\dot{x}_i - \dot{x}_{lead}) + q_4(x_i - x_{lead} - \sum_{j=0}^{i} L_i) \tag{5.34}$$

As with the speed control task above, the objective is satisfied when $S_{ui} = 0$, so we drive the system to this surface by defining

$$\dot{S}_{ui} = -\lambda_u S_{ui} \tag{5.35}$$

Again, solving for a_{isynth} as a synthetic control yields:

$$a_{isynth} = \frac{\ddot{x}_{i-1} - q_1 \dot{\epsilon}_i + q_3 \ddot{x}_{lead} - q_4 (\dot{x}_i - \dot{x}_{lead}) - \lambda_u S_{ui}}{(1 + q_3)} \tag{5.36}$$

In the case of a single follower (which corresponds to the experimental set-up), the follower law reduces to:

$$S_u = (1+q_3)\dot{\epsilon} + (q_1+q_4)\epsilon \tag{5.37}$$

$$a_{synth} = \ddot{x}_{lead} - \frac{(q_1+q_4)}{(1+q_3)}\dot{\epsilon} - \frac{\lambda_u}{(1+q_3)}S_u \tag{5.38}$$

As mentioned above, this follower law is by no means unique. Indeed, other researchers have proposed alternate rules for maintaining constant spacing as well as strategies that maintain constant (or speed-dependent) time headways (see, for instance, (Ioannou and Xu, 1994)). Such strategies can also be formulated in terms of the synthetic input, a_{synth}, (Hedrick *et al.*, 1993) and therefore simply represent another possible choice for S_u.

5.3.3 Platoon Joining and Splitting

(Connolly and Hedrick, 1996) demonstrated that the platoon joining and splitting tasks can be put into the same form as the speed tracking law above. Here, however, the desired velocity is not solely a function of time, but also a function of the current spacing and the "lead" vehicle acceleration and velocity (in this context, the lead vehicle is taken to be the car immediately preceding the merging or splitting vehicle). The exact formula for calculating this velocity involves passenger comfort limits as well as safety concerns and, hence, is somewhat involved. As a result, the reader is referred to (Connolly and Hedrick, 1996) for a discussion of joining and splitting and experimental validation of these control laws with the coordinated throttle and brake controller presented here.

5.4 Throttle and Brake Switching Criterion

Finally, we complete the control structure by transforming the synthetic input, a_{synth}, from the upper surface controller into the desired brake and engine torques, τ_{bdes} and τ_{edes}. Central to this development is a switching element that determines whether engine or brake control is required. This switch is presented in Section 5.4.1 as a logical consequence of the vehicle dynamics.

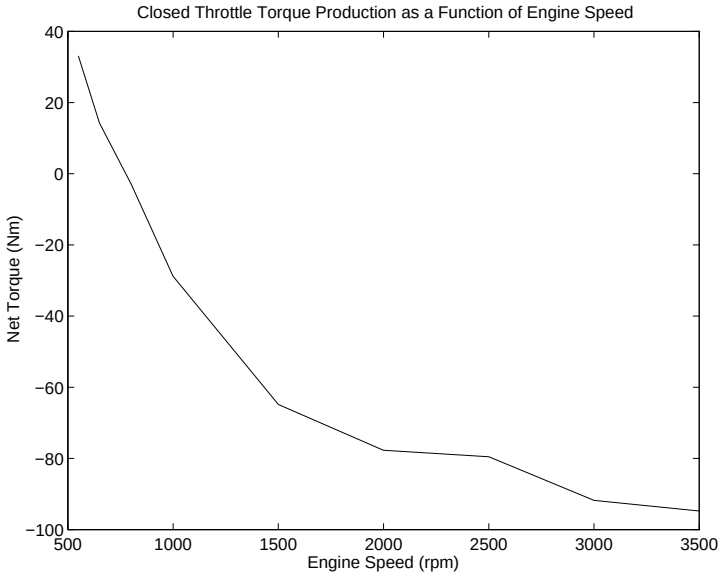

Figure 5.6: Closed Throttle Torque Production

5.4.1 Closed Throttle Behavior and Switching

Section 5.1.2 described the behavior of the engine when the throttle angle is set to zero and illustrated how the closed-throttle behavior defines the lower edge of the engine map. While Figure 5.5 projected this edge into the $\omega_e - P_{man}$ plane, we can also think of this as producing a minimum torque, described by the projection into the $\omega_e - \tau_e$ plane. This function is illustrated in Figure 5.6. The physical interpretation is that the engine, in the absence of throttle input, will decay to this curve and remain on it, producing a torque which depends solely upon engine speed.

This brings to light a certain distinction between the engine and brake torques in vehicle motion; namely, that some engine torque is always produced. As a result, the engine torque can be divided into two parts: the minimum - or closed-throttle - torque, τ_{ect}, and the portion subject to control, τ_{ec}. In this interpretation, τ_{ec} represents the height above the lower edge in the engine map of Figure 5.2.

Breaking the engine torque into these two components and substituting

into Equation 5.16 gives

$$\tau_{ec} - R_g \tau_b = \beta a + R_g \left(M_{rr} + hF_a + mgh \sin\theta \right) - \tau_{ect} \tag{5.39}$$

Note that the two torques on the left hand side, τ_{ec} and τ_b, are non-negative by definition. Hence, Equation 5.39 can be used to form a simple switching condition between brake and throttle control. Defining the residual acceleration in the absence of control inputs,

$$a_{resid} = \frac{1}{\beta} \left[\tau_{ect} - R_g (M_{rr} + hF_a + mgh \sin\theta) \right] \tag{5.40}$$

the switching criterion becomes

$$a_{synth} \geq a_{resid} \implies \text{Throttle Control} \tag{5.41}$$

$$a_{synth} < a_{resid} \implies \text{Brake Control} \tag{5.42}$$

Once the control action has been chosen, the desired torque is given by

$$\tau_{edes} = \beta a_{synth} + R_g \left(M_{rr} + hF_a + mgh \sin\theta \right) \tag{5.43}$$

for throttle control and

$$\tau_{bdes} = -\frac{(\beta a_{synth} + \tau_{ect})}{R_g} - (M_{rr} + hF_a + mgh \sin\theta) \tag{5.44}$$

for brake control.

Physically, the conditions in Equations 5.41 and 5.42 state that a desired acceleration greater than that due to the drag terms and closed-throttle engine torque requires throttle control; acceleration less than this requires braking. Graphically, this condition may be treated as a function of desired acceleration and the current vehicle speed, as demonstrated in Figure 5.7. This figure shows the switching criterion for the experimental test vehicle while in 3rd gear with the interpretation that points above the solid line necessitate throttle control and those below require brakes.

Any time a switching interface exists in a control system, the potential for chatter exists. Physically, such chatter can result from noise in the signal used to determine the switch, finite sampling rate, and discrepancies between the modeled and actual values of the interface, among other factors.

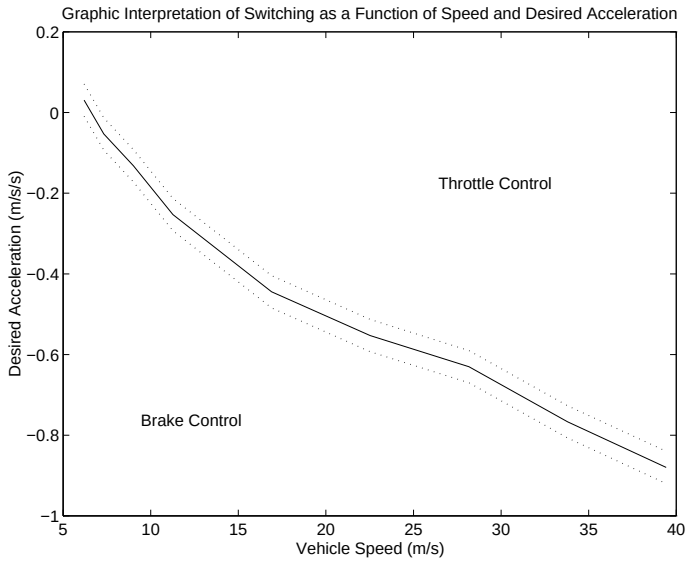

Figure 5.7: Switching Condition for 3rd Gear Operation

Accordingly, introducing a small hysteresis about the interface (as indicated by the dotted lines of Figure 5.7) is often useful from an implementation standpoint. Unfortunately, including a hysteresis element can also confound analysis of the system, preventing a clear treatment of its effects on tracking or other performance benchmarks. In the case of the vehicle controller, such analysis is possible.

Since this switching rule depends only upon one of the vehicle states (namely, v) and the desired acceleration, it is completely independent of the various upper surfaces described in the previous section. Hence, this control structure meets the stated goal of being transparent to the upper surface. Secondly, the switching rule is unambiguous; accelerations above those due to system drift can simply not be achieved without throttle control. Finally, the switching prevents simultaneous application of the brakes and throttle. Such application - in a longitudinal sense - serves no purpose and utilizes unnecessary control activity since the engine torque and brake torques cancel each other out.

It should be noted that while this switching condition can be easily described mathematically, there is one obstacle to implementation. In order

to calculate the residual acceleration in Equation 5.40, some measurement of the road grade, θ is necessary. Unfortunately, such a measurement is not currently available on the experimental test vehicles. Since the test tracks used for experimentation were relatively flat, the grade changes were simply treated as a disturbance to which the controller is robust. The magnitude of the grade term, however, precludes the use of such a strategy over the range of road grades currently found on highways. Because multi-axis accelerometers currently being developed for automotive applications possess the ability to determine the direction of gravity (Ajluni, 1995), this is considered to be only a temporary obstacle.

5.4.2 Comparison With Other Switching Rules

The longitudinal controllers of (Hedrick *et al.*, 1991), (Hedrick *et al.*, 1993) and (Choi and Devlin, 1995) have all based the switch between throttle and brake control on the throttle surface dynamics. Specifically, the use of either throttle or brakes was determined from the the value of α calculated in Equation 5.28:

$$\begin{array}{rcl} \alpha & \geq & 0 \implies \text{Throttle} \\ \alpha & < & 0 \implies \text{Brake} \end{array} \tag{5.45}$$

There are two problems with such an approach, however. From an implementation standpoint, the desired throttle angle is a much noisier signal than either a_{synth} or a_{resid} as a result of the pressure transients illustrated in Figure 5.5. Hence, considerable chatter occurs around the switching interface under this rule.

More fundamentally, however, switching based upon the desired throttle angle fails to recognize the partition illustrated in Figure 5.7. At a given speed, clearly, the choice of input needed to produce a given acceleration is unique. Switching around the throttle angle, however, bases the decision upon the *rate of change* of the desired acceleration and not the magnitude. This not only causes switching to occur at a frequency corresponding to the engine dynamics (which are faster than the vehicle longitudinal dynamics) but also precludes even a qualitative prediction of the system performance. Indeed, the system switches to brake control when the throttle input saturates at zero, regardless of whether there even exists a level of brake torque corresponding to the desired acceleration.

Despite the problems with this approach, it does raise an interesting point regarding the speed of the engine and brake dynamics. Clearly, even if these dynamics are excluded from the switching criterion, they cannot be omitted from the analysis. Neither the engine torque nor the brake torque can be decreased arbitrarily rapidly, so some residual brake torque will exist after the switch to throttle control and vise versa. These issues are considered explicitly in the more rigorous treatment of switching.

An alternate switching criterion in the context of vehicle following was proposed by (Ioannou and Xu, 1994). This switching logic based the choice of throttle or brakes upon the distance and closing rate between the vehicle and the preceding car. As a result, the idea cannot be easily extended to speed control, platooning with lead vehicle information or the joining and splitting of platoons, so direct comparison is not terribly meaningful. Like the controller presented here, the switching logic included a hysteresis element to avoid chatter.

5.5 Simulation Results

To confirm the suitability of the controller structure presented here, a series of simulations was performed. The results, described in the sections that follow, provide some compelling evidence that the coordinated throttle and brake controller is indeed capable of tracking both speed and desired spacing. Furthermore, inclusion of the hysteresis element in the switching condition is shown to introduce only a small tracking error. While these simulations, taken alone, do not conclusively prove anything, the combination of these results with the switching theory and the experiments comprises a rather complete validation.

The parameters used in the simulations, except where noted, can be found in Table 5.1. For all of the results shown here, the vehicle transmission was locked in 3rd gear and the hysteresis size was set at 0.05 m/s^2. As with the brake control simulations, these simulations incorporated a fourth-order Runge-Kutta integration algorithm with a fixed step size of 1 millisecond and a controller loop time of 10 milliseconds.

$m = 2148\,\text{kg}$	$M_{rr} = 72.6\,\text{Nm}$	$\theta = 0$	$q_1 = 1.0$
$\beta = 234\,\text{kgm}$	$C_a = 0.5334\,\text{kg/m}$	$\lambda_u = 1.5$	$q_3 = 0.5$
$h = 0.33\,\text{m}$	$R_g = 0.326$	$\lambda_e = 10$	$q_4 = 0.5$

Table 5.1: Parameters Used in Coordinated Control Simulations

5.5.1 Speed Control

Figure 5.8 shows the results of a speed tracking test where the desired velocity was produced from a trapezoidal acceleration profile. Clearly, both the manifold pressure and brake pressure (the solid lines) track their desired values (indicated by the dashed lines) quite closely. Accordingly, the actual and desired vehicle velocities are essentially indistinguishable (the peak error is less than 0.015 m/s). Note that the transition between throttle control and brake control is quite smooth and the tracking error produced by the hysteresis is almost imperceptible.

However, as Figure 5.9 indicates, this particular trajectory produces a synthetic input, a_{synth}, that spends very little time in the hysteresis band around a_{resid}. Hence, it is not terribly surprising that the hysteresis produces little tracking error. While this may, in fact, be a desirable trait for trajectory design, it does little to illuminate the effect of the hysteresis. More appropriate is a test such as that illustrated in Figure 5.10, which produces a synthetic input that remains in the hysteresis band for over two seconds.

Yet, as indicated in Figure 5.11, tracking error in this case is also quite small, with a peak below 0.02 m/s. Analytically, if the engine and brake torques could be controlled directly, hysteresis of width Φ would result in a maximum tracking error of Φ/λ_u, as a result of the sliding control structure. For the numerical values is this simulation, that translates to a rather miniscule error of 0.034 m/s. Of course, in the presence of model uncertainty, manifold dynamics and brake fluid dynamics, the analysis becomes somewhat more involved. However, the effects of the hysteresis can be made smaller than those naturally due to uncertainty, thereby guaranteeing that the hysteresis does not influence the tracking bound.

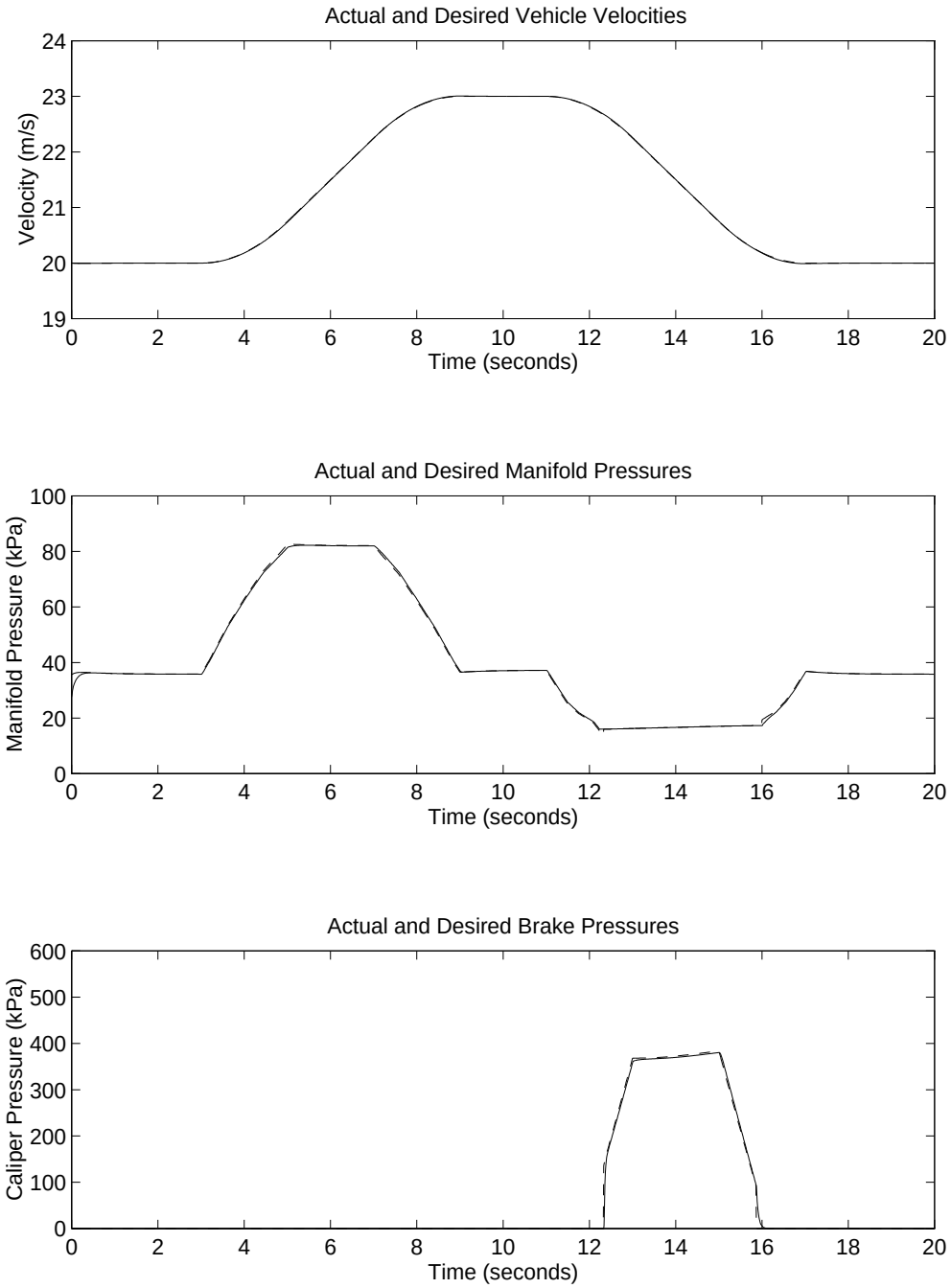

Figure 5.8: Speed Control (Desired - dashed, Actual - solid)

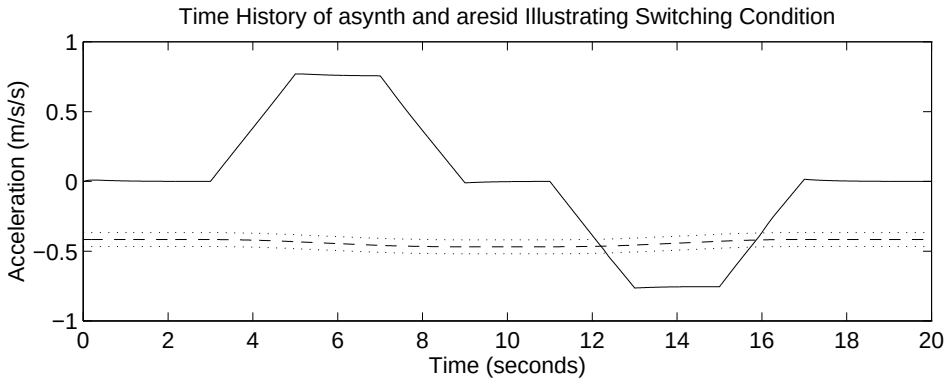

Figure 5.9: Switching Behavior During Speed Control

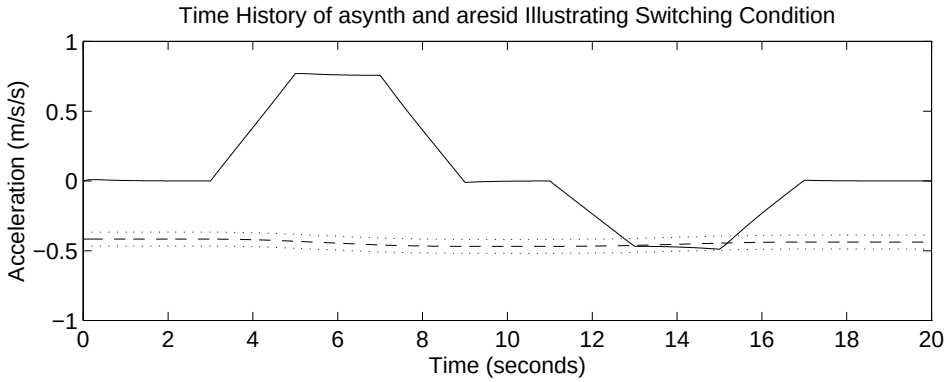

Figure 5.10: Switching Behavior During Speed Control - Low Deceleration

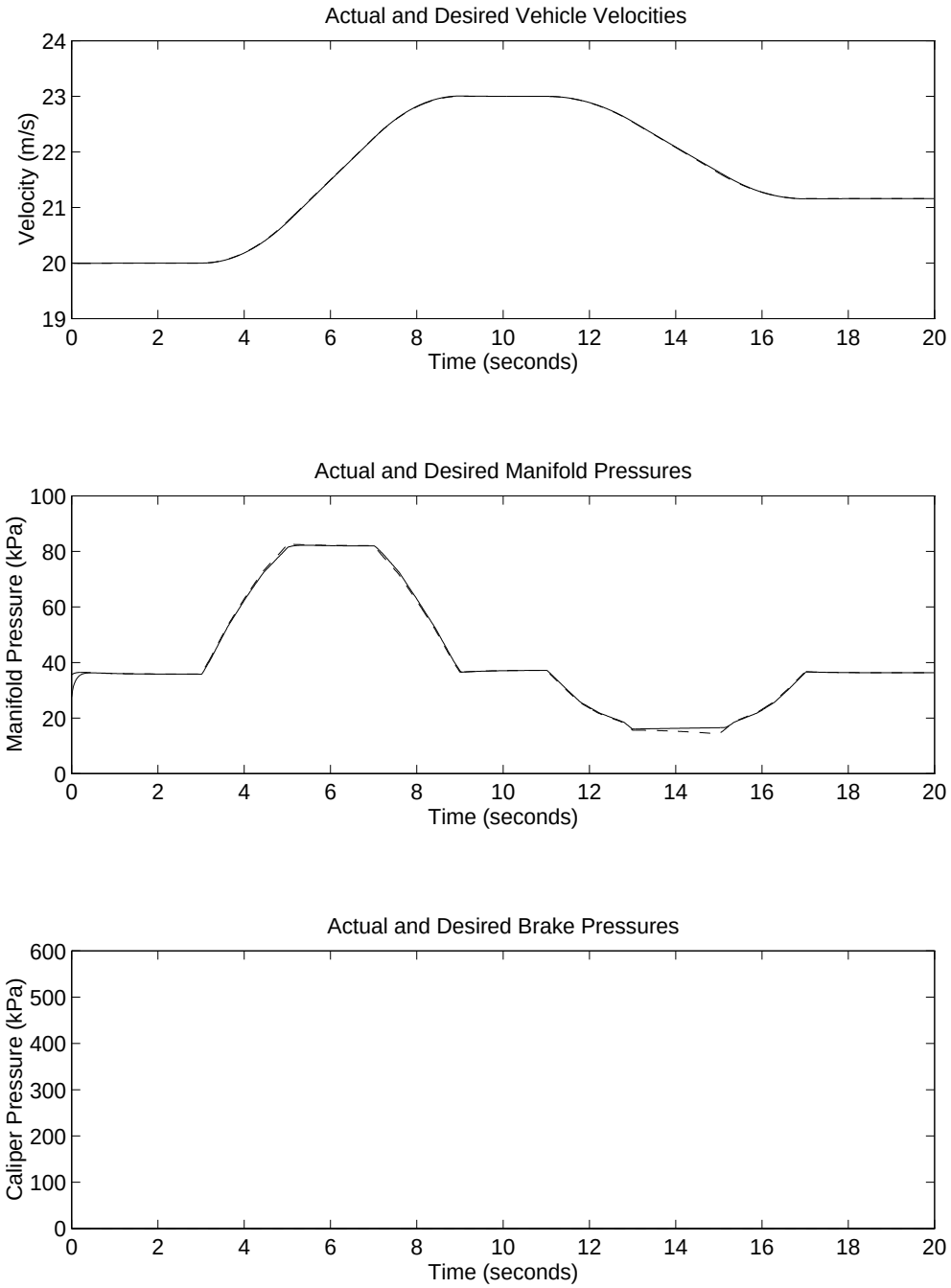

Figure 5.11: Speed Control: Low decel. (Desired - dashed, Actual - solid)

5.5.2 Spacing Control

Two types of simulations were run to evaluate the spacing control law. In the first type, the lead vehicle was assumed to follow a computer-generated trajectory, comparable to that used for the desired speed, $v_{des}(t)$, in Figure 5.8. In the second type, the lead vehicle was assumed to operate under the speed control law, so the following car "sees" a more volatile signal. Since all of these results are generated in simulation, this might seem to be a rather unnecessary distinction. From an experimental standpoint, however, these are very different tests, so separate simulations are indeed useful as a basis for comparison. Furthermore, in experiment, the upper surface gain, λ_u, was reduced to 0.75 in tests involving two cars in order to compensate for the additional sensor noise; the simulations presented here reflect that reduction.

Figure 5.12 shows the computer-generated lead vehicle trajectory along with the resulting synthetic input for the follower. Since $\ddot{x}_l$ is the dominant component of a_{synth}, these two plots exhibit a considerable likeness both to each other and to the speed tracking test in Figure 5.9 (where a_{synth} is dominated by the same signal, in the form of $\dot{v}_{des}$). Consequently, as demonstrated by Figure 5.13, the desired manifold and brake pressures strongly resemble those illustrated in Figure 5.8. As in the speed tracking tests, tracking of the manifold and brake pressures is quite accurate, resulting in a peak spacing error of less 1 centimeter.

When the lead vehicle information is taken from the output of a vehicle follower task as opposed to being generated directly, slight changes can be observed in $\ddot{x}_l$. As shown in Figure 5.14, the hysteresis results in small "notches" in the lead acceleration which propagate through to a_{synth}. Little difference can be seen in the desired manifold or brake pressures, illustrated in Figure 5.15. Furthermore, the spacing error looks almost identical to that pictured in Figure 5.13, although magnified by a factor of two to reflect the gain reduction in λ_u. Figures 5.16 and 5.17 present results for a similar test where the level of deceleration has been increased from 0.75 m/s^2 to 2 m/s^2. While not a panic stop, this trajectory definitely falls outside the limits of normal automated highway operation. Nevertheless, tracking is still quite good.

One other aspect to be mentioned briefly is the concept of string stability. As discussed by (Swaroop, 1994), one objective in the design of controllers for

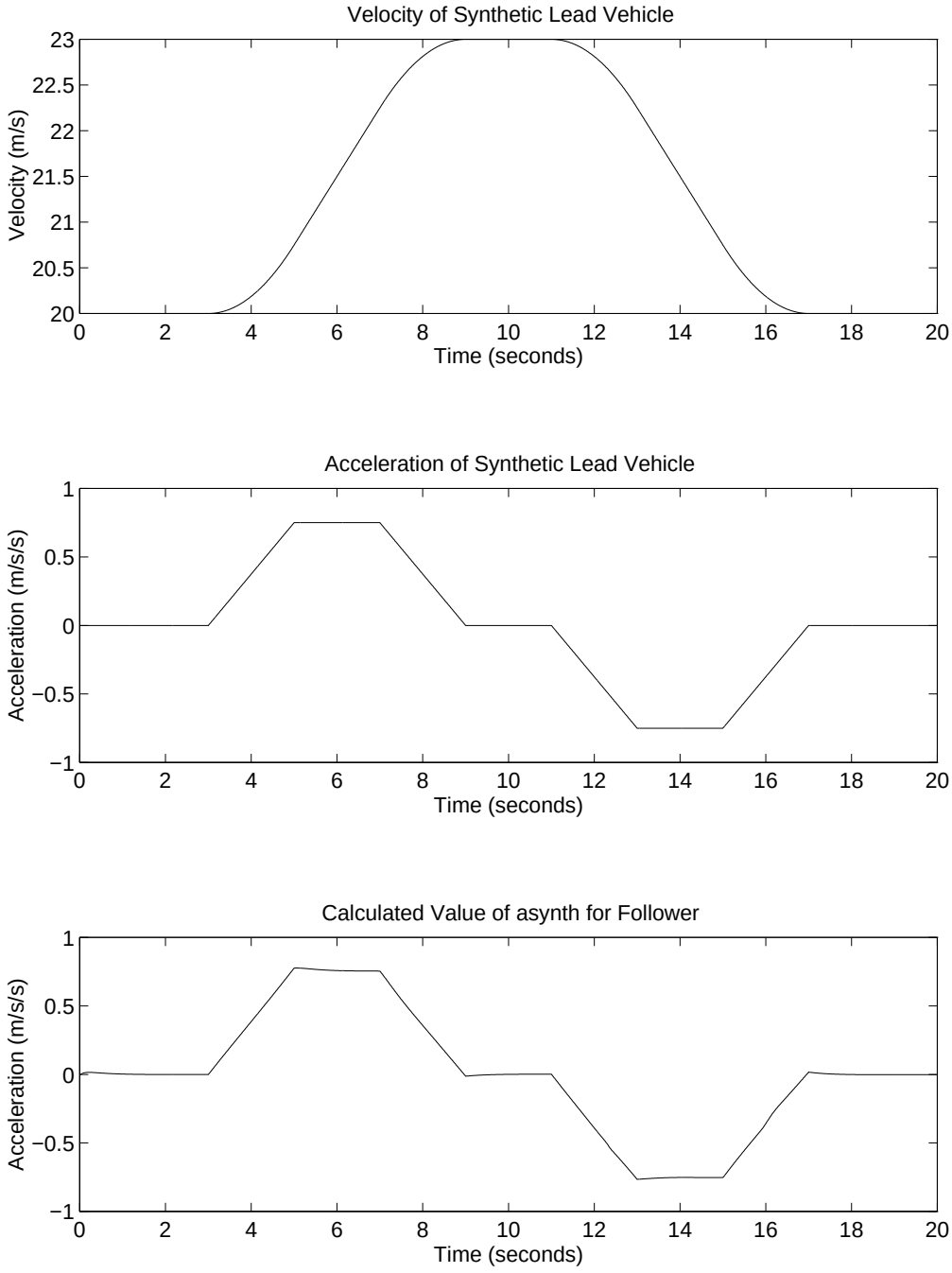

Figure 5.12: Follower Law Test with Synthetic Lead Vehicle - Trajectory

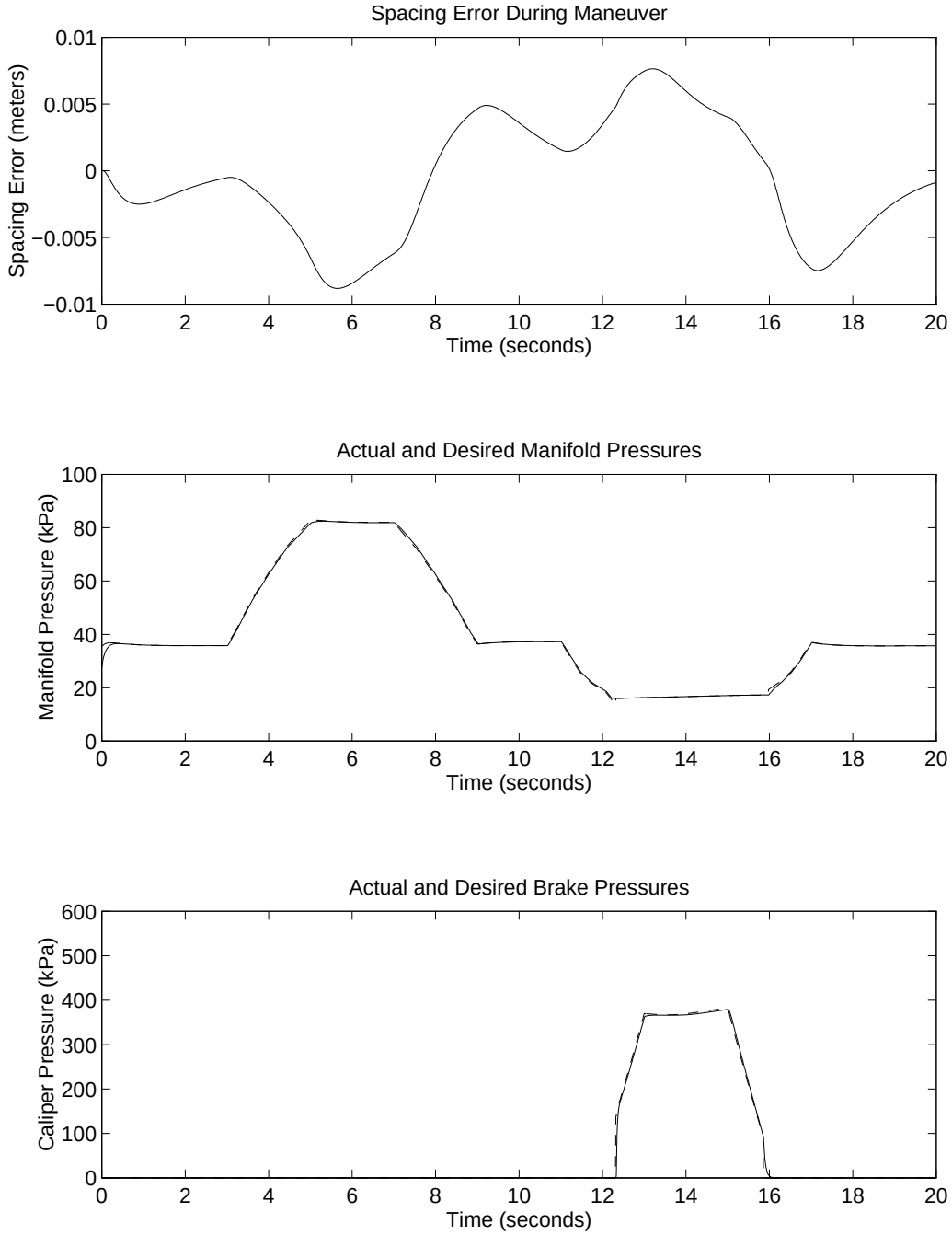

Figure 5.13: Follower Law: Synthetic Lead (Desired - dashed, Actual - solid)

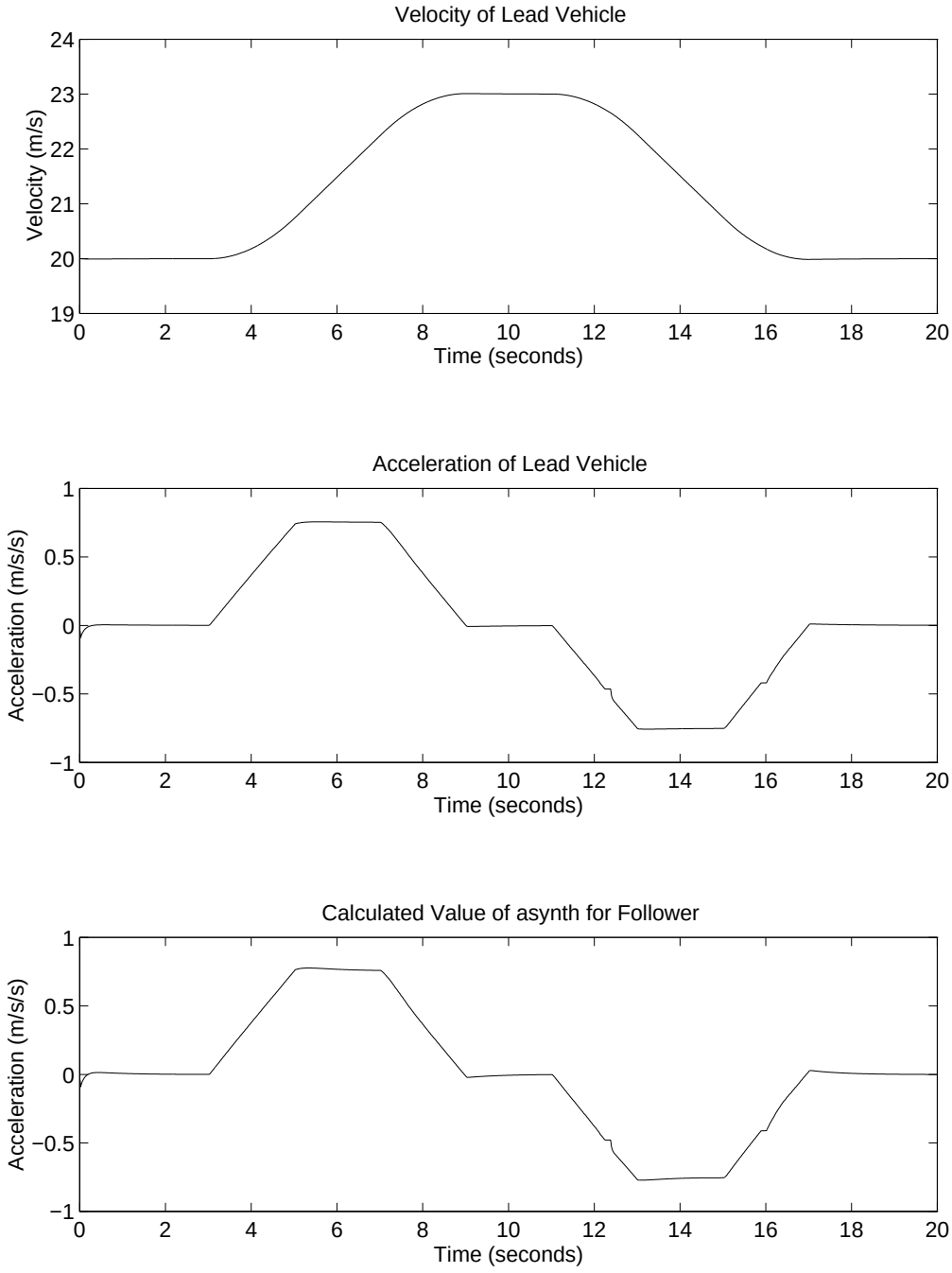

Figure 5.14: Follower Law Test with Lead Vehicle - Trajectory

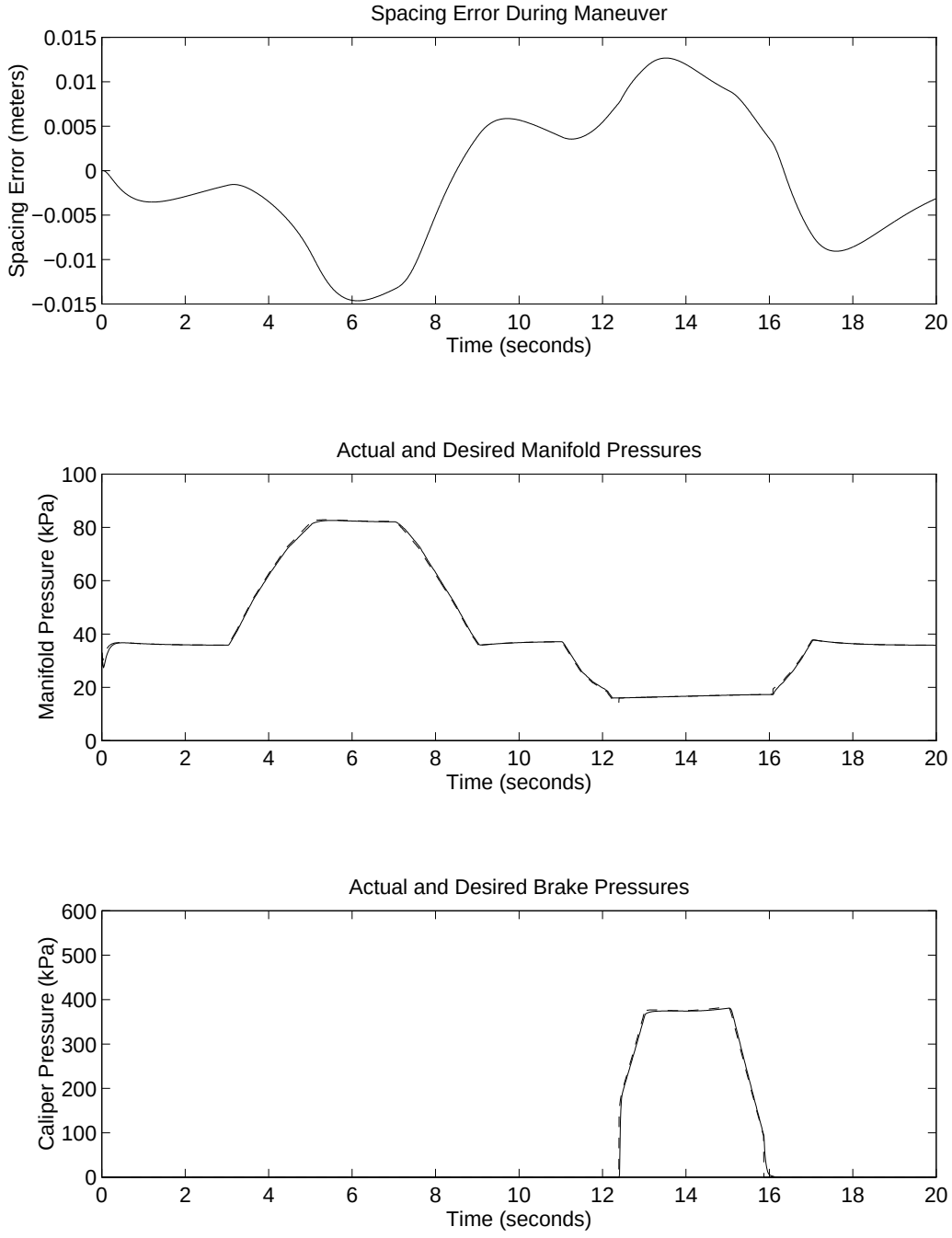

Figure 5.15: Follower Law: Lead Vehicle (Desired - dashed, Actual - solid)

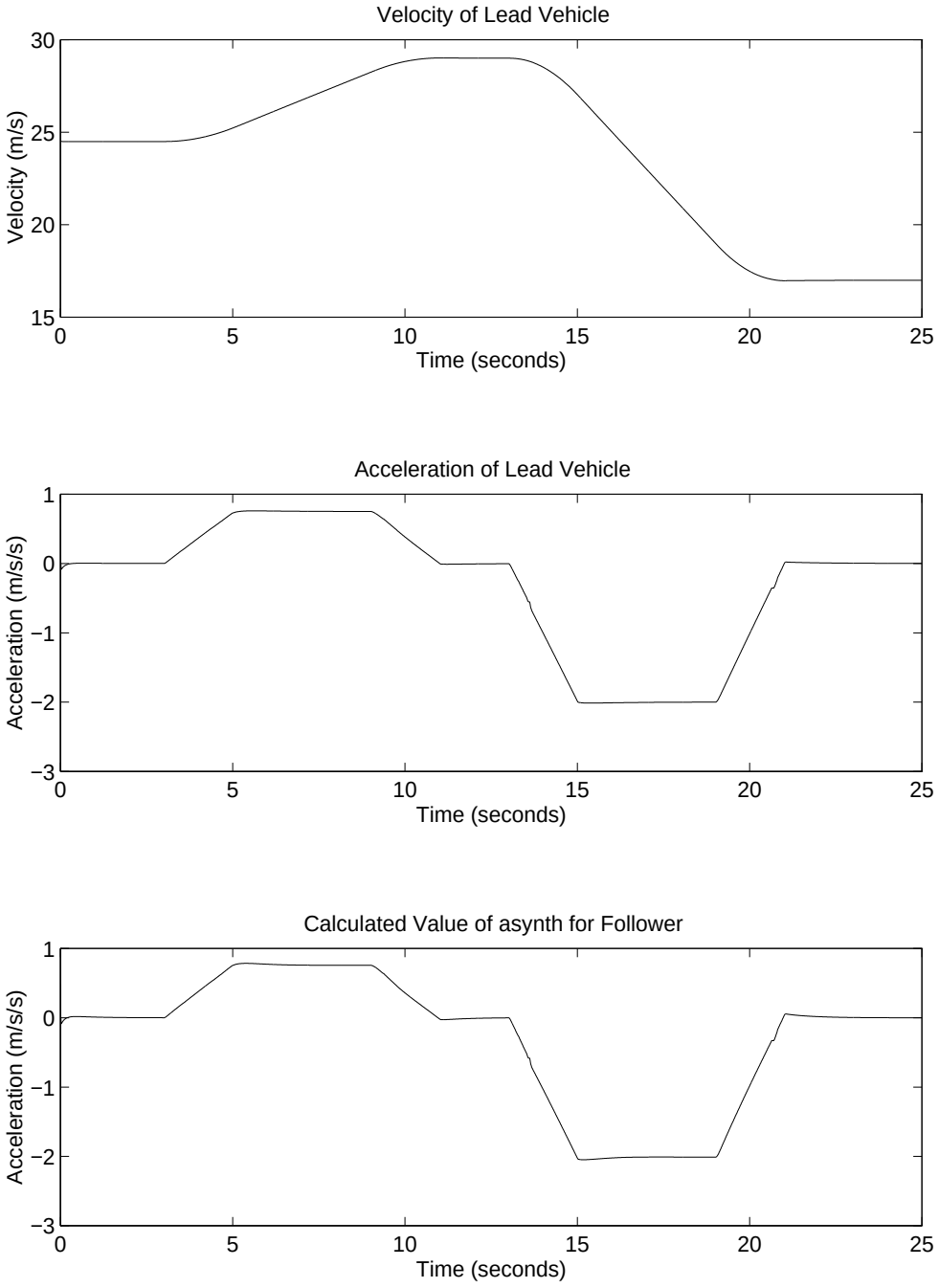

Figure 5.16: Extreme Follower Law Test with Lead Vehicle - Trajectory

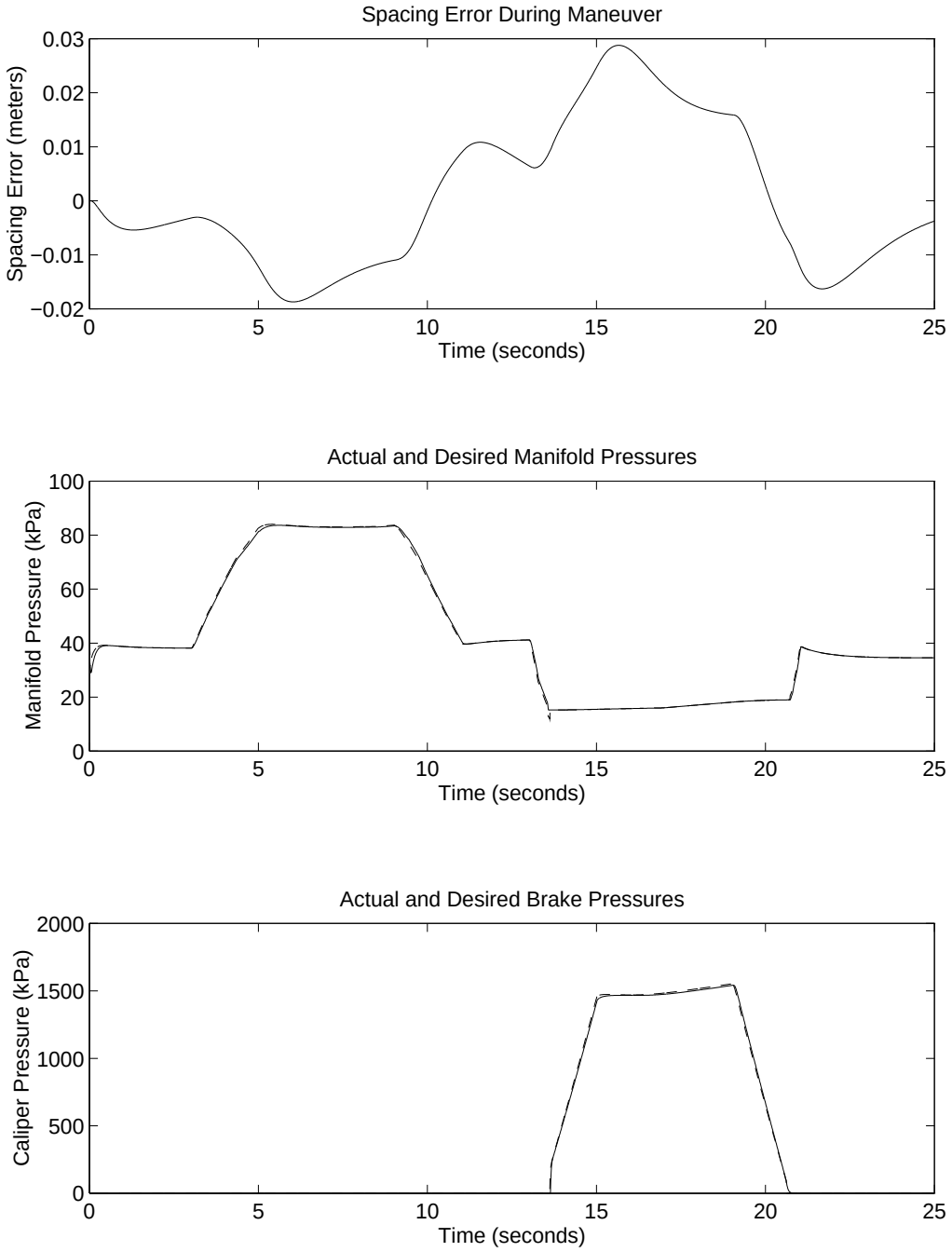

Figure 5.17: Follower Law: Extreme with Lead (Desired - dashed, Actual - solid)

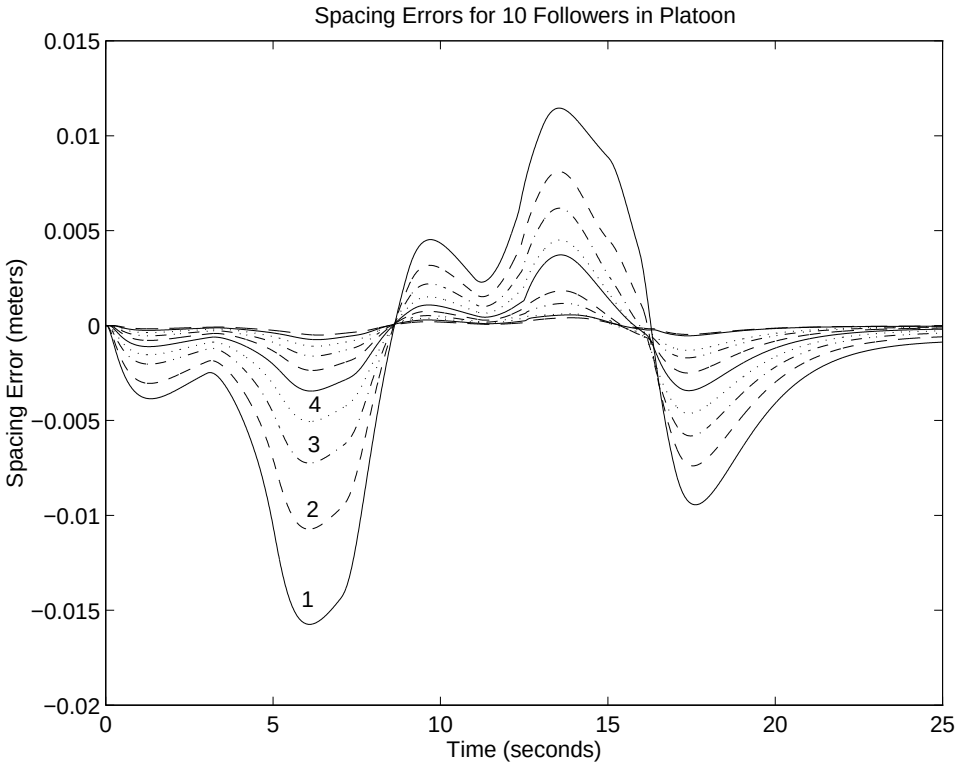

Figure 5.18: Spacing Errors for Platoon with 10 Followers

platoons of automated vehicles is for the spacing error resulting from a lead vehicle maneuver to decrease as the platoon is traversed. In other words, the resulting spacing error for each vehicle should be less than that for the vehicle which precedes it. To achieve this, the q_i for the upper surface controller were chosen according to the criteria for string stability in (Swaroop, 1994). While a theoretical treatment of string stability for the entire system with engine dynamics, brake dynamics and hysteresis is beyond the scope of this work, Figure 5.18 indicates that the basic property still holds. Indeed, each successive following car exhibits progressively less error in response to the lead car maneuver illustrated in Figure 5.12.

Chapter 6

Conclusions

This report presented a three-state model of brake dynamics which, despite its simplicity, meets or exceeds the accuracy of previous models. Furthermore, aspects critical to control design, such as hysteresis and disturbance modeling are explicit in this formulation. Current implementation issues with this system include incorporating a nonlinear first-order model of the brake hydraulics into the sliding controller and eliminating undesired switching between throttle and brakes due to sensor noise.

As mentioned previously in the text, the class of systems used in developing the DSC structure includes the normal form used for backstepping design, prompting a comparison between the two methods. From the standpoint of complexity, the dynamic surface controller is the clear winner; conversely, the backstepping approach offers the mathematical appeal of global results. Due to the severe constraints inherent in the vehicle dynamics, global results were not relevant to the application, however global results can be developed by imposing stricter Lipschitz requirements on the system dynamics and adopting a more conservative, Lyapunov-based approach to design. Unfortunately, this design process loses the intuitive appeal of the results presented here.

A method to estimate the coefficient between the brake pressure at the wheel and the brake torque was presented. An experimental setup to directly measure the brake torque was also presented. Verification experiments are scheduled.

The choice of hysteresis width in the design procedure of the switching

controller was motivated solely by the effect on the tracking error bound. Experimentally, this hysteresis was also shown to remove chatter across the switching interface. Guaranteeing that such chatter reduction occurs, however, is an open issue. Furthermore, it is a very difficult issue, involving some characterization of sampling time effects and sensor noise. Nevertheless, the problem of chatter in switched systems is very fundamental and a theoretical understanding of the effects of hysteresis in eliminating such concerns would be extremely powerful.

Bibliography

Ajluni, Cheryl (1995). Accelerometers: Not just for airbags anymore. *Electronic Design* pp. 93–106.

Buschmann, G., M. Roth and K. Saalbach (1993). Tandem master cylinder in change - due to specific requirements of Anti Lock and Traction Control Systems. SAE Paper # 930504.

Cho, D. and J. K. Hedrick (1989). Automotive powertrain modeling for control. ASME *Journal of Dynamic Systems, Measurement, and Control* **111**, 568–576.

Choi, S. B. and P. Devlin (1995). Throttle and brake combined control for intelligent vehicle highway systems. SAE Paper # 951897.

Connolly, T. R. and J. K. Hedrick (1996). Longitudinal transition maneuvers in an automated highway system. Submitted to 1996 ASME IMECE.

Fisher, D. K. (1970). Brake system component dynamic performance measurement and analysis. SAE Paper # 700373.

Gerdes, J. C. and J. K. Hedrick (1995). Brake system requirements for platooning on an automated highway. In: *Proceedings of the 1995 American Control Conference, Seattle, WA.* pp. 165–169.

Gerdes, J. C., D. B. Maciuca, J. K. Hedrick and P. E. Devlin (1993). Brake system modeling for IVHS longitudinal control. In: *Advances in Robust and Nonlinear Control Systems,* ASME *Winter Annual Meeting.* pp. 119–126.

Gillespie, Thomas D. (1992). *Fundamentals of Vehicle Dynamics.* Society of Automotive Engineers. Warrendale, PA.

Hedrick, J. K., D. H. McMahon and D. Swaroop (1993). Vehicle modeling and control for automated highway systems. Technical Report UCB-ITS-PRR-93-24. California PATH Program.

Hedrick, J. K., D. McMahon, V. Narendran and D. Swaroop (1991). Longitudinal vehicle controller design for IVHS systems. In: *Proceedings of the 1991 American Control Conference, Boston, MA*. pp. 3107–3112.

Ioannou, P. and Z. Xu (1994). Throttle and brake control systems for automatic vehicle following. *IVHS Journal* **1**(4), 345–377.

Khan, Y., P. Kulkarni and K. Youcef-Toumi (1994). Modeling, experimentation and simulation of a brake apply system. ASME *Journal of Dynamic Systems, Measurement, and Control* **116**, 111–122.

Limpert, Rudolf (1992). *Brake Design and Safety*. Society of Automotive Engineers. Warrendale, PA.

Maciuca, D. B., J. C. Gerdes and J. K. Hedrick (1994). Automatic braking control for IVHS. In: *Proceedings of the International Symposium on Vehicle Control*.

McMahon, D. H., J. K. Hedrick and S. E. Shladover (1990). Vehicle modelling and control for automated highway systems. In: *Proceedings of the 1990 American Control Conference, San Diego, CA*. pp. 297–303.

McMahon, D. H., V. K. Narendran, D. Swaroop, J. K. Hedrick, K. S. Chang and P. E. Devlin (1992). Longitudinal vehicle controllers for IVHS: Theory and experiment. In: *Proceedings of the 1992 American Control Conference, Chicago, IL*. pp. 1753–1757.

Moskwa, J. J. and J. K. Hedrick (1987). Automotive engine modeling for real time control application. In: *Proceedings of the 1987 American Control Conference*.

Motor Auto Repair Manual, Volumes 1 and 2 (1991). 55th ed.

Motor Imported Car Repair Manual, Volumes 1 and 2 (1991). 13th ed.

Nash, R. (1983). Brake integrated hydraulic actuation system master cylinder. SAE Paper # 830412.

Puhn, Fred (1985). *Brake Handbook*. HP Books. Los Angeles, CA.

Radlinski, R. W. (1991). The effect of aftermarket linings on light vehicle braking performance. Final Report DOT HS 807 835. U.S. Department of Transportation, NHTSA.

Raza, H., Z. Xu, P. Ioannou and B. Yang (1994). Brake modeling for AVCS application. Report. California PATH Program.

Shevitz, Daniel and Brad Paden (1993). Lyapunov stability theory of nonsmooth systems. In: *Advances in Robust and Nonlinear Control Systems*. Vol. 53. ASME. New Orleans, LA. pp. 53–60.

Swaroop, D. and J. K. Hedrick (1994). Direct adaptive control of vehicle platoons. In: *Proc. 33rd CDC, Lake Buena Vista, FL*. pp. 684–689.

Swaroop, D. V. A. H. G. (1994). String Stability of Interconnected Systems: An Application to Platooning in Automated Highway Systems. PhD thesis. University of California at Berkeley.

van Zanten, Anton T., Rainer Erhardt and Georg Pfaff (1995). VDC, the vehicle dynamics control system of Bosch. SAE Paper # 950759.

Xu, Z. and P. Ioannou (1992). Modeling of the brake line pressure to tire brake force subsystem. Technical Report 92-09-01. California PATH Program.